Research Paper

GEOSPHERE

GEOSPHERE, v. 14, no. 4,

https://doi.org/10.1130/GES01609.1

16 figures; 1 table

CORRESPONDENCE: hodei@geol.uniovi.es

CITATION: Uzkeda, H., Poblet, J., Bulnes, M., and Martín, S., 2018, Effects of inherited structures on inversion tectonics: Examples from the Asturian Basin (NW Iberian Peninsula) interpreted in a Computer Assisted Virtual Environment (CAVE): Geosphere, v. 14, no. 4, p. 1635–1656, https://doi.org/10.1130/GES01609.1.

Science Editor: Raymond M. Russo
Associate Editor: Francesco Mazzarini

Received 31 August 2017
Revision received 16 March 2018
Accepted 30 April 2018
Published online 30 May 2018

Effects of inherited structures on inversion tectonics: Examples from the Asturian Basin (NW Iberian Peninsula) interpreted in a Computer Assisted Virtual Environment (CAVE)

Hodei Uzkeda[1,*], Josep Poblet[1,*], Mayte Bulnes[1,*], and Santiago Martín[2,*]

[1]Departamento de Geología, Universidad de Oviedo, C/Jesús Arias de Velasco s/n, 33005 Oviedo, Spain
[2]Departamento de Construcción e Ingeniería de Fabricación, Universidad de Oviedo, Campus de Viesques, Edificio Departamental no. 6, 33203 Gijón, Spain

ABSTRACT

Two outcrops in the Asturian Basin (northwest Iberian Peninsula) composed of Lower–Middle Jurassic alternations of limestones and marls, including black shales proven to be hydrocarbon source rocks, were analyzed from a structural point of view. In both outcrops, an inversion tectonic event of Cenozoic age caused contractional folds and faults, as well as a change in the structural style up section, superimposed on previous Mesozoic extensional structures. However, the mode and kinematic evolution of the inversion tectonics were very different; folding predominated in one of the outcrops, whereas faulting is the most important phenomenon in the other one. The characteristics of the two coastal outcrops (irregular surface, inaccessible portions, accessibility restricted to low tide periods, good quality of rock exposure and scale) led us to build virtual outcrop models using photogrammetry (structure from motion) and interpret them in a computer-assisted virtual environment (CAVE). The analysis of both field data and the virtual outcrop model–derived results (three-dimensional models and cross sections) allowed us to conclude that mechanical stratigraphy and the type, characteristics, and distribution of previous structures were the key factors that controlled the inversion tectonic mode. Awareness of their influence should help when trying to understand inversion structures in similar geological settings.

INTRODUCTION

The Asturian Basin constitutes a portion of the North Iberian continental margin originated during extensional Permian–Mesozoic events, subsequently subjected to inversion tectonics during a Cenozoic contractional event (Fig. 1A). The Permian–Mesozoic evolution of this basin initiated after the Variscan orogeny of Carboniferous age and culminated with the opening of the Bay of Biscay. The Cenozoic history is linked to the Alpine orogeny, which involved the convergence of the Iberian and European plates. Currently, the southern portion of the Asturian Basin is emerged and crops out in the northwest part of the Iberian Peninsula, whereas the north part of the basin is submerged under the waters of the Cantabrian Sea. In the subaerial portion of the basin, many Jurassic rocks crop out (Fig. 1A), especially along the coastal areas, where their exposure is, in many cases, excellent. Because of this, the stratigraphy and sedimentology of these rocks have been intensely studied (e.g., Suárez Vega, 1974; Valenzuela et al., 1986; Valenzuela, 1988; García Ramos and Gutiérrez Claverol, 1995; and many others), and they have also been studied from other points of views, such as: hydrogeology, hydrocarbons, jet jewelry, dinosaur paleontology, geological engineering, and geological heritage (see, for instance, Soler et al., 1981; Menéndez Casares et al., 2004; Lockley et al., 2007; and many others). The main structural features of the Asturian Basin have been described in regional studies, some involving geological mapping (e.g., Beroiz et al., 1972a, 1972b, 1972c; Pignatelli et al., 1972), whereas others have focused on establishing the structural framework of portions of the basin (e.g., Lepvrier and Martínez García, 1990; Uzkeda, 2013; Alonso, 2014; Odriozola, 2016; Uzkeda et al., 2016). However, despite the exceptional outcrops along the coastline, there are only a few of detailed studies of individual structures (e.g., Uzkeda et al., 2013). We examined here two excellently exposed outcrops of faulted and folded Jurassic rocks, where the variations in the rock competence along the stratigraphic succession triggered different structural styles, and where different types of inversion tectonics are exhibited. Our research focused on the mechanisms by which and extent to which inherited structures influenced inversion tectonics. The studied outcrops, which are meter- to decameter-scale features, are located by the Cantabrian Sea along the shoreline of the Principality of Asturias, Spain, and they belong to the northernmost part of the onshore portion of the Asturian Basin (Figs. 1B and 1C).

Although the quality of the two studied outcrops is exceptional, their morphology, characterized by inlets and protrusions due to the marine erosion of the coastal cliffs, makes it very difficult to construct undistorted geological

*E-mails: hodei@geol.uniovi.es, jpoblet@geol.uniovi.es, maite@geol.uniovi.es, martinsantiago@uniovi.es

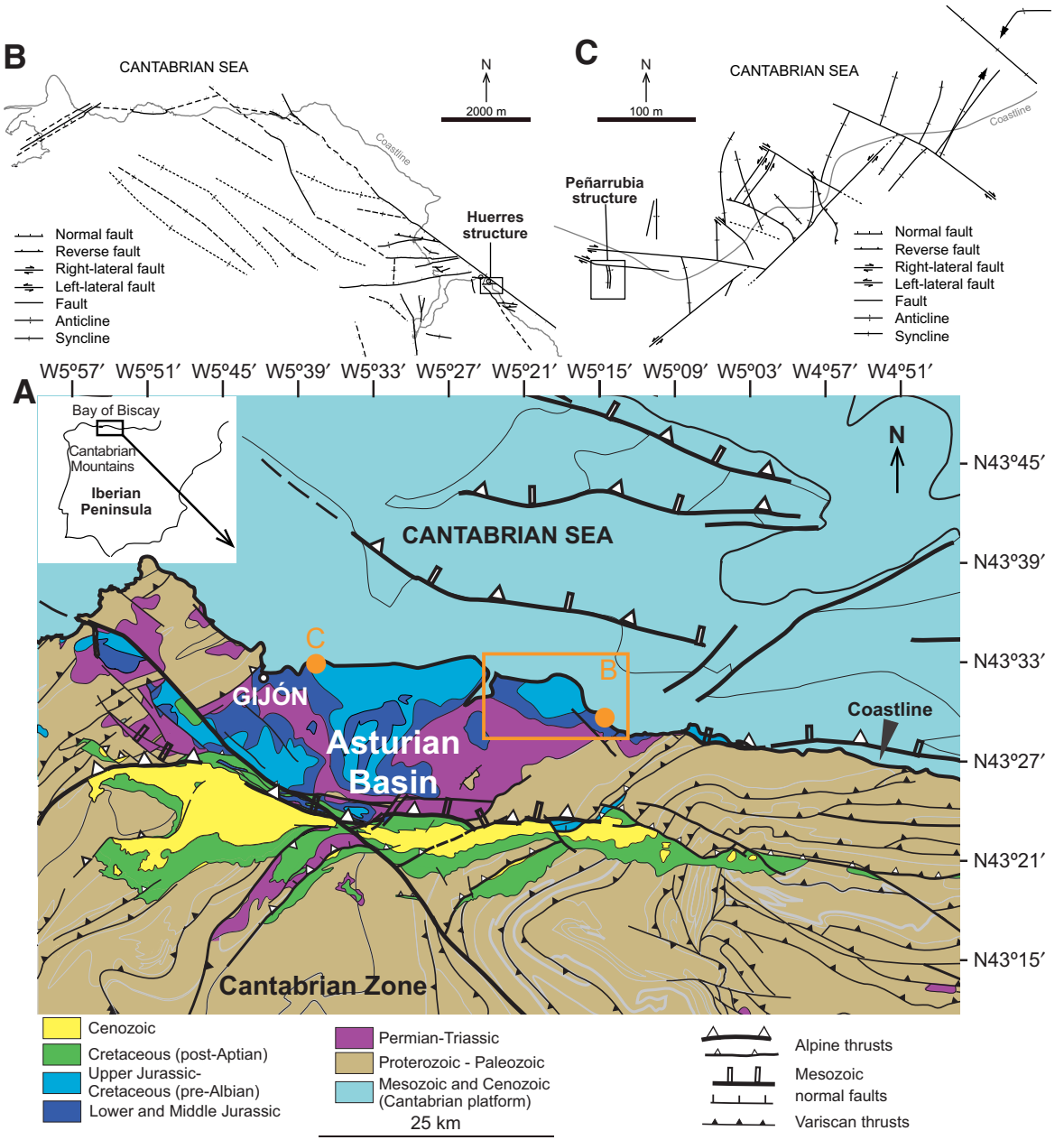

Figure 1. (A) Geological map of the Asturian Basin (modified from Alonso et al., 2009) and structural sketches of the surrounding areas of the two studied outcrops: (B) Huerres (modified from Uzkeda et al., 2016) and (C) Peñarrubia (modified from Odriozola, 2016).

interpretations. In addition, some portions of the outcrops are not accessible due to their steep slopes, and the outcrops can only be visited during low tide periods. Thus, deciphering the main features and understanding the kinematics of the two selected examples required a remote three-dimensional (3-D) approach. The strategy chosen consisted of conventional field work together with construction of a virtual outcrop model in the form of a point cloud following the structure from motion system (Fig. 2) and subsequent analysis. High-dynamic-range photographs of the outcrops, georeferenced using a total station and differential global positioning system (GPS), were used. The resulting model was visualized in a computer-assisted virtual environment (CAVE) and geologically interpreted using in-house software called the 3-D Stereo Virtual Drawing Tool (3D Stereo VDT). The 3-D geological data sets obtained were the basis for 3-D geological models from which geological cross sections were constructed.

Using the 3-D structural models and the detailed geological cross sections, the main features of the different structures developed in the outcrops were unraveled, and the distribution of folds and faults was analyzed in order to establish their relationships with previous structures and with the competence contrast of the rocks, and also to characterize the variation in structural style up section conditioned by the presence of detachments within the stratigraphic succession. On the other hand, the influence of folding and fracturing on uplift and shortening was quantified, a structural evolution was proposed for each field example analyzed, and finally the similarities and differences between them were examined.

GEOLOGICAL SETTING

The different fold and fault sets that control the present-day configuration of the Asturian Basin developed during extensional regimes from the late Paleozoic to Mesozoic and during a Cenozoic contractional event (e.g., Pello, 1967; Julivert et al., 1971, 1973; Gervilla et al., 1973a, 1973b; Pignatelli et al., 1973; Suárez Vega, 1974; Suárez Rodríguez, 1988; Lepvrier and Martínez-García, 1990; Alonso et al., 1996; Rodríguez Fernández et al., 1996; Pulgar et al., 1999; Alonso and Pulgar, 2004; Uzkeda, 2013; Uzkeda et al., 2013, 2016; Alonso, 2014; Odriozola, 2016). The Permian, Mesozoic, and Cenozoic sediments that fill in this basin lie unconformably over a Cambrian to Carboniferous basement, which was involved in a foreland fold-and-thrust belt of the Variscan orogen of west Iberia known as the Cantabrian zone (Fig. 1A). These basement rocks belong to the north branch of the Ibero-Armorican or Asturic orocline, responsible for the arching of the Variscan orogen in the western portion of the Iberian Peninsula. The events recorded in the basin infill that crop out in the onshore portion of the Asturian Basin reflect continental rifting during Permian–Triassic times, followed by a thermal subsidence period, possible extensional thermal doming during the Middle Jurassic, a remarkable subsidence period, and an extensional event in the Late Jurassic–Cretaceous. In Cenozoic times, the Asturian Basin was partially inverted.

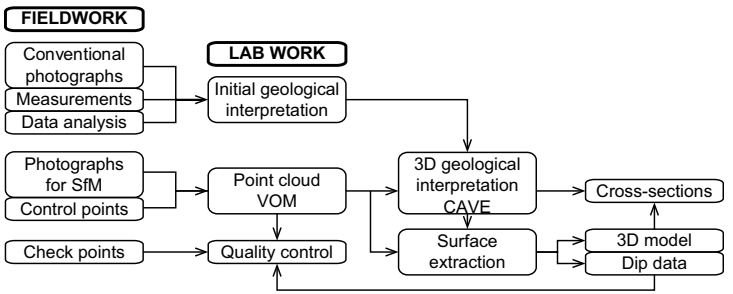

Figure 2. Proposed workflow from the collection of field data to the construction of sections across the studied structures using the strategy presented here. SfM—structure from motion, VOM—virtual outcrop model, CAVE—computer-assisted virtual environment, 3D—three dimensional.

The field examples analyzed here involve the Rodiles Formation, divided into the Buerres and Santa Mera Members (Valenzuela et al., 1986), the ages of which range from upper Sinemurian to lower Bajocian, i.e., Lower to Middle Jurassic (Suárez Vega, 1974). This stratigraphic unit consists of an ~110–210-m-thick alternation of gray marls and limestones with abundant fossil remains such as bivalves, gastropods, brachiopods, echinoderms, belemnites, ammonites, reptiles, fishes, and trace fossils, amongst others (Valenzuela et al., 1986), deposited in a carbonate ramp. There are also some levels of black shales (García-Ramos et al., 1992, 2001; Suárez-Ruiz and Prado, 1995; Bádenas et al., 2013), the high organic matter content of which indicates hydrocarbon source rocks with type II kerogen (Soler et al., 1981; Valenzuela et al., 1986; Valenzuela, 1988; Suárez-Ruiz and Prado, 1995; Riaza Molina, 1996; García-Ramos et al., 2008; Bádenas et al., 2013).

The first example, the Huerres structure, crops out in the north-northeast portion of the emerged portion of the Asturian Basin (Fig. 1B). In this region, the major folds are open, upright, and relatively rounded and exhibit NW-SE strikes, and the major faults are normal and have three predominant orientations: NW-SE, NE-SW, and E-W. Evidence of selective and irregularly distributed inversion tectonics has been recognized. Thus, some normal faults were reactivated as reverse or strike-slip faults, whereas others display buttressing effects. They may also be deformed due to next-generation structures, such as thrusts, which usually display E-W strikes (Uzkeda, 2013).

The second example, the Peñarrubia structure, is located in the northern part of the emerged portion of the Asturian Basin (Fig. 1C). The main structural features of its surrounding area consist of two generations of major open to gentle, upright, and rounded folds: an older set with NE-SW trends and a younger one with NW-SE trends. Three systems of faults, with strikes of NE-SW, NW-SE, and E-W, have been identified. Most kinematic indicators on the fault planes indicate strike-slip movement; however, some normal and reverse faults also occur. Locally, N-S structures appear (Odriozola, 2016).

The existence of superimposed tectonic events makes it highly important to understand how inversion took place and which parameters conditioned the

process, for instance, in order to determine whether mechanical stratigraphy and the different manners in which previous structures reacted to a younger tectonic event (being reactivated, remaining as passive elements, or constraining the distribution of deformation) may lead to a situation where folding is dominant over faulting. These two outcrops, the rocks of which have undergone similar tectonic events but exhibit different rheological properties and inherited structures, are key features that can be used to decipher the control exerted by these factors on the inversion tectonics.

METHODOLOGY

The framework of the investigation was to characterize the geometry and kinematics of the analyzed structures using a combination of field work and laboratory-based tasks aimed at extracting 3-D information and generating accurate cross sections (Fig. 2).

This method has a number of advantages:

(1) A CAVE offers a proper 3-D view of the outcrops, in contrast to virtual outcrops visualized in computer screens, which are based on perspectives or contrasts between light and shadows and different colors used to simulate a 3-D view, and, therefore, it makes the interpreter feel as if they are really in the field.

(2) Virtual outcrop views in computer screens are usually small and require the interpreter to move and rotate the image, as well as enlarge it and reduce it, to properly interpret their geological features. Conversely, working inside a CAVE does not require so many operations to carry out a geological interpretation because its large size allows an overview of the outcrop, reducing the need to navigation around the model.

(3) Like with other techniques of analysis of virtual outcrops, it is possible to obtain distortion-free 3-D geological data, to analyze the whole outcrop, even portions hardly accessible in the field, and it allows us to "bring the outcrop to the laboratory," where it can be visualized and analyzed using different geological tools, and where it can be shared at any time.

Field Work: Acquisition of the Photographs and Control and Check Points

It is recommended to take photographs of the outcrops with as much quality as possible. One key point is to employ large depths of field to make sure that everything is in focus. Furthermore, the employment of techniques such as high dynamic range helps to increase the quality by overcoming lighting problems such as shadowed areas. In addition, it also helps to take all the photographs with the same camera, in particular, a fixed-focus lens camera. A summary of recommendations for photographs of field outcrops may be found in Martín et al. (2013). Regarding the number of photographs, a minimum of three images for each feature is required. However, the higher the number of photographs, the better is the outcome, i.e., the denser the point cloud will be. The Huerres outcrop was covered with 60 photographs, whereas the Peñarrubia outcrop required 63 images. It is also recommended that the photographs have enough overlap. In some cases, two sets of photographs—one set covering the whole area from relatively far away, and a second one from a closer distance, focused on some especially important details (i.e., minor fractures, intersections between structures, tension gashes, etc.)—supply better results. For instance, in the field examples studied here, closer photographs were taken covering the areas with the highest density of structures, such as the southern limb of the Huerres anticline and the forelimb of the Peñarrubia anticline. It is advisable to take photographs covering the whole outcrop from different angles and positions (ideally, surrounding the element of interest), which should prevent any gaps produced by areas obscured or not visible from a certain location or shooting trajectory.

Using a combination of total station and differential GPS, accurate coordinates of control points (employed to georeference the point cloud) and check points (not used for building the point cloud, but for testing its quality) must be taken in the field. These points might be either targets placed with such purpose in strategic positions on the outcrop and/or, as was the case in the examples described below, natural points such as intersections between beds and joints, changes in rock color, significant topographic features, etc. Three is the minimum number of points needed, although the result may improve if more points are employed. These points should be taken evenly spread along the outcrop, cover the whole scene, and be distributed at different depths of view.

All these tasks must be accompanied by conventional field work, which ought to include: geological mapping; measurement of orientation of planes and lines of interest, such as bedding, fractures, fold axes, and kinematic indicators; measurement of lengths, such as fault displacements and bed thickness; geological sketch drawing; taking of conventional oriented photographs and photogeological interpretation; and structural analysis of the collected data. All this information should be the foundation on which to carry out an initial geological interpretation of the area under study. In the examples shown in this paper, a geological map and a conventional photogeological interpretation were constructed to serve as the basis for the following analysis. This, together with some field sketches, helped with the interpretation of especially complicated areas within the CAVE. In addition, bedding and fault orientation were measured.

Creation of the Virtual Outcrop Model: Point Cloud

A point cloud with associated color information (*x*-*y*-*z* red-blue-green [RGB] files) may be created, as in this study, using the software VisualSFM (downloadable for free at http://ccwu.me/vsfm; Wu, 2013), which works following the structure from motion system developed by Wu et al. in 2011 (for applications of structure from motion in earth sciences, see Carrivick et al., 2016; see also Fig. 2). This software solves the problem of the camera calibration

(calculation of focal length, center of projection, radial distortion), as well as of resection (determining the camera positions for each photograph). This is done by the bundle adjustment method (Triggs et al., 2000; Wu et al., 2011), with automatic detection of matching points using the Scale Invariant Feature Transform algorithm. Had the camera been calibrated before, it is also possible to load the corresponding parameters and set a fixed calibration in VisualSFM. Since the camera used in this research had not been calibrated, the first approach was followed. The different available options are: (1) downsampling the point cloud for large-scale interpretation when not so much detail is needed, which should cause better computer performance; (2) dividing the point cloud into smaller portions to be analyzed independently; (3) deleting areas without interest; and (4) obtaining a textured triangulated mesh. Given that the chosen outcrops were of relatively manageable size, the downsampling and the extraction of small portions were not necessary. However, some zones of no interest, such as fallen blocks at the bottom of the cliffs, were removed. Moreover, no triangulated meshes were created, given that they were not necessary for the research.

Georeferencing the Point Cloud

This step consists of placing the point cloud in its correct geographical position and with its appropriate orientation and dimensions. This is a vital issue, since it allows proper 3-D coordinates to be obtained for the geological features interpreted in the point cloud, as well as measuring plane and line orientations. To carry out this step, coordinates of control points along the studied area must be used. This step may be carried out using the software VisualSFM with a minimum of three points. To estimate the error, the point to point comparison method may be used (Fonstad et al., 2013), which consists of using check points recorded in the field and left out of the point cloud generation procedure (Fig. 2). It should also help to detect outliers that must be removed from the model. For the Huerres outcrop, six control points plus 16 check points were taken, whereas the Peñarrubia example was covered with six control points and 18 check points.

Visualization and Geological Interpretation in a CAVE

The in-house software 3-D Stereo VDT, developed by the research group IdeasCAD (University of Oviedo), was used to visualize and interpret the point cloud from the geological point of view within a CAVE (Fig. 2). This software combines shutter glasses and a handheld device to pick features from the point cloud. Infrared cameras track the position of the user to provide the correct view of the outcrop and that of the drawing tool, and to draw the geological features at their accurate position. 3-D Stereo VDT software allows the user to draw points and polylines, as well as to edit, delete, or modify them. It also allows the use of different colors and widths to distinguish different beds, faults, joints, fold axes, and many other sets of geological features. The geological interpretation carried out in the CAVE must be based on the initial geological interpretation performed during the field data collection. This preliminary interpretation helps to provide a broad outline of the structure and determine the areas of special interest. Thus, the geologist has an idea of the main characteristics of the structure and can focus on drawing it as precisely as possible within the CAVE. In the examples shown here, the conventional photogeological interpretations were used to define the horizons and faults that were going to be interpreted on the point cloud. The geological interpretation may be exported as a dxf file, which can be imported in most conventional drawing or geological software programs to continue its analysis, i.e., construction of geological cross sections, restorations, etc. For instance, the interpretations of the examples presented in this paper carried out in the CAVE were loaded in the software Move (Midland Valley Exploration Ltd., Glasgow, UK) to continue with the analysis and generate the 3-D model and the different cross sections shown. Although the software was implemented in a CAVE, it could also be adapted to more affordable systems such as head-mounted displays (Oculus Rift or HTC Vive). However, this is beyond the scope of this study.

Given that the software 3-D Stereo VDT works with "obj" files, and VisualSFM only generates "ply" files, it is necessary to change the file format. This can be achieved, as, indeed, was done in this research, using the open source tool MeshLab (available for free at http://meshlab.sourceforge.net/), wherein it is also feasible to remove unneeded areas or select only those parts of interest. It should be borne in mind that 3-D Stereo VDT cannot handle more than around five million points. In case of point clouds with more points, MeshLab allows two strategies to overcome this issue: (1) Reduce the density of the whole point cloud by applying the Poisson-disk sampling algorithm (Corsini et al., 2012), which implies losing some minor details, and/or (2) divide the point cloud into smaller parts that can be loaded separately. Fortunately, the point clouds created from the outcrops studied here did not exceed this limit.

Surface Extraction: 3-D Model and Geological Cross-Section Building

The data interpreted in the previous step must be extracted (Fig. 2). From various selected points on a surface, it is possible to calculate the surface mean dip and dip direction or strike. These estimated values may be compared to those directly measured in the field using a conventional compass and/or an electronic device such as a mobile telephone or tablet, as a way to check the accuracy of the point cloud. Dips and strikes may also be obtained for areas otherwise inaccessible, such as the highest parts of the outcrops, in order to fill gaps in the conventional mapping.

The lines interpreted in the point cloud, and subsequently extracted, may be projected onto selected planes to create geologically meaningful cross sections. These lines may also be used to produce surfaces by extending them while observing constraints such as the strike and dip of bedding and of

structural elements (fold limbs, fold axes, and fault surfaces), and honoring dip domains. This procedure may be carried out using commercial 3-D geomodeling software such as Skua-Gocad (Paradigm Geophysical B.V.) or Move (Midland Valley Exploration Ltd.), amongst others, in order to construct a 3-D geological model. For the research presented here, surfaces were built using Move, and they were then used to generate geological cross sections perpendicular to the axes of the structures.

HUERRES STRUCTURE

The Huerres structure is located near the small village of Huerres, around 30 km to the east of Gijón (Figs. 1A and 1B). The structure crops out along a coastal cliff that is ~50 m wide and around 60 m high, although the studied structure is restricted to the lower 5–10 m. The average orientation of the cliff face is NNW-SSE; however, the structure is located at a small salient (Fig. 3A).

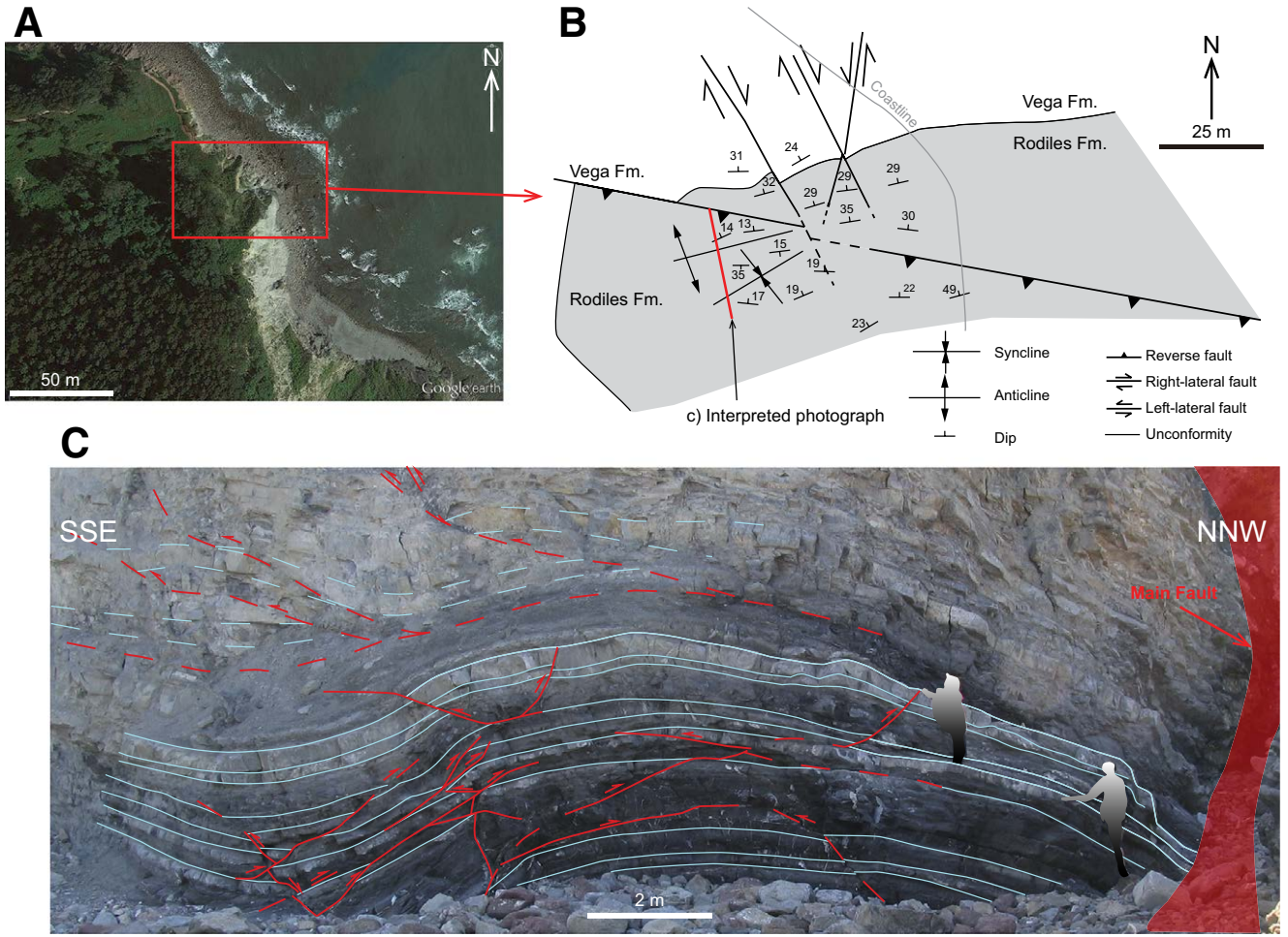

Figure 3. (A) Google Earth image with location of the geological map illustrated in B. (B) Geological map of the Huerres outcrop and surrounding areas. See Figure 1 for location of this map within the Asturian Basin. (C) Photograph of the Huerres outcrop along with its geological interpretation. The structure involves alternations of gray limestones and marls, and black shales and limestones (Santa Mera Member, Rodiles Formation). Black shales and marls predominate in the lower part of the outcrop, whereas gray limestones predominate in the upper part. Blue lines—bedding, red lines—faults.

The field work carried out allowed us to construct a geological map (Fig. 3B), as well as a photogeological interpretation of the outcrop (Fig. 3C), and projections of the collected orientation data (Fig. 4). Sixty high-dynamic-range photographs of the outcrop were shot, and 22 control and check points were taken (Fig. 5A). The point cloud (Fig. 5B), georeferenced using six control points, was interpreted from a geological point of view (Fig. 6A) with the help of field observations. This interpretation, together with the orientation data for the layers and structural elements, allowed us to develop a 3-D geological model (Fig. 6B), from which a geological section perpendicular to the fold axes was constructed (Fig. 6C). The mean square error estimated from comparing the coordinates of the check points measured in the field with their location in the point cloud was 8.5 cm. In addition, we estimated the strike and dip of eight bedding surfaces located in different places of the point cloud. The obtained values were compared with measurements of strike and dip taken directly at the outcrop at the same locations. The average angle between the bedding planes calculated using the point cloud interpretation and the bedding planes measured in the field varied from 4° to 14°, average 11°. These discrepancies are similar to those obtained by Cawood et al. (2017) when comparing orientations measured in the field with those of fitted surfaces extracted from point clouds created by photogrammetry (terrestrial and aerial structure from motion) in areas where it is possible to achieve an adequate coverage (i.e., good overlap, resolution, no occlusion, etc.). Taking into account the possible errors due to the irregularity of the bedding surfaces, those derived from the measurement instruments, and those made by ourselves in the interpretations and

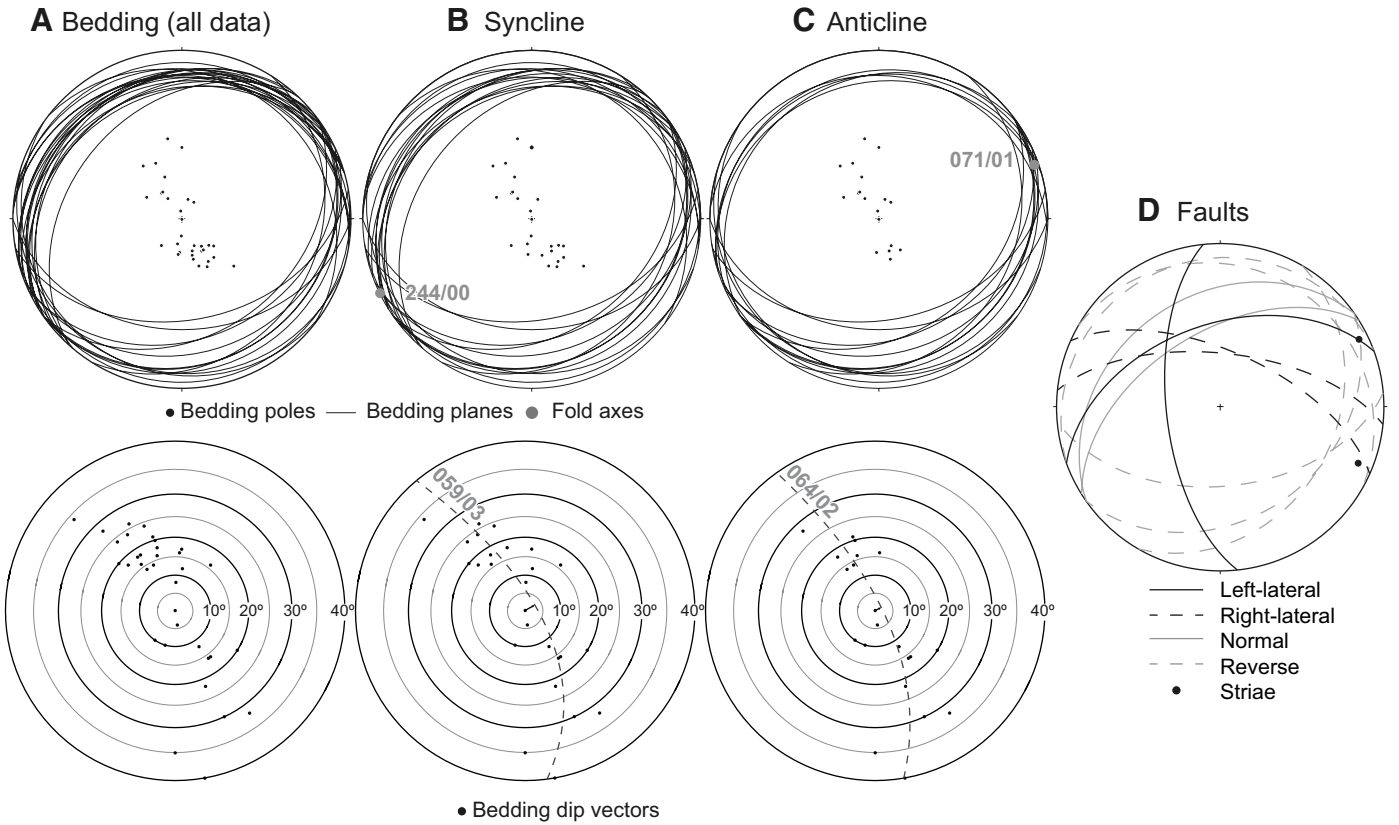

Figure 4. Equal-area projections in the lower hemisphere and tangent diagrams of orientation data collected in the Huerres outcrop. (A) Bedding (surfaces and poles); (B) bedding (surfaces and poles) and average fold axis for the syncline; (C) bedding (surfaces and poles) and average fold axis for the anticline; and (D) faults, along with their kinematic indicators. Equal-area projections were plotted using the software Stereonet. Tangent diagrams have 5° increments. The bedding dip vectors displayed in the tangent diagrams have been fitted using a quadratic function.

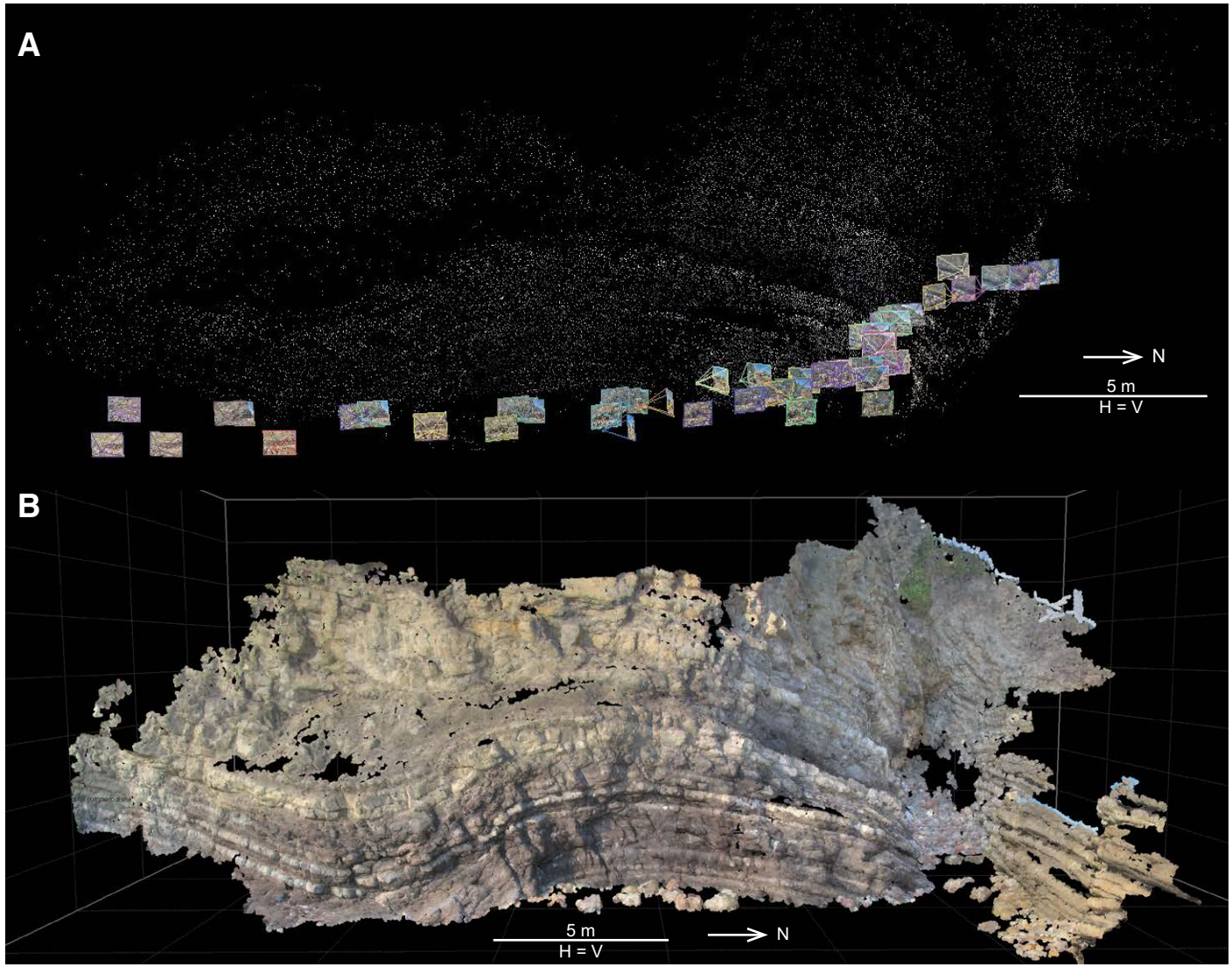

Figure 5. (A) High-dynamic-range photographs employed to construct the virtual outcrop model of the Huerres outcrop in the form of a point cloud, displayed in (B). The software VisualSFM was used to construct the point cloud. H—horizontal, V—vertical.

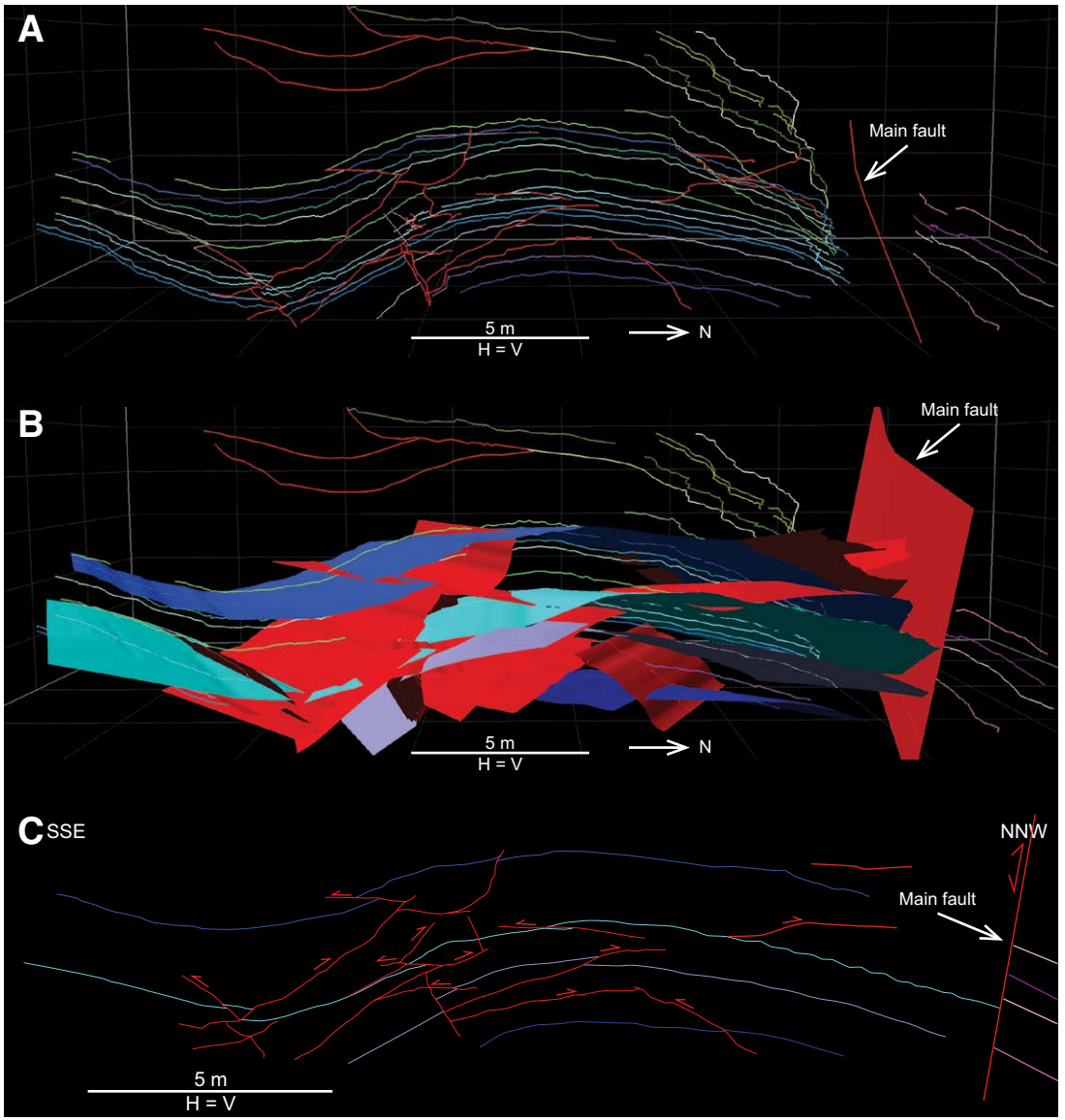

Figure 6. (A) Three-dimensional (3-D) geological interpretation of the Huerres point cloud displayed in Figure 5B carried out with the software 3-D Stereo VDT in a computer-assisted virtual environment (CAVE). (B) 3-D geological model of the Huerres outcrop constructed using the software Move, field data, and the CAVE interpretation shown in A. (C) Geological section across the lower portion of the Huerres structure obtained from the 3-D geological model displayed in B. Red lines and surfaces—faults, other color lines and surfaces—bedding, H—horizontal, V—vertical.

measurements, we consider that the errors obtained from the check points and from the orientations of bedding surfaces support the accuracy of the point cloud constructed for geological purposes.

Structural Features

The most noticeable structure identified in the Huerres outcrop consists of a decameter-scale, approximately parallel syncline and anticline pair (Figs. 3, 5B, and 6). These folds are gentle to open, and their interlimb angles are ~120° (Fig. 4). The anticline width measured from the syncline hinge to its intersection with a fault to the north is ~15 m, and its structural relief is around 2 m (Fig. 6C). The north limb of the anticline dips gently to the NNW, whereas its south limb, which is the common limb with the syncline, is shorter than the north limb and dips a little bit steeper to the SSE. The south limb of the syncline again dips gently to the NNW. The fold axes and axial surfaces of these folds have an ENE-WSW direction, and they are approximately upright structures (Fig. 4). However, the anticline is a little vergent toward the SSE. These folds are slightly conical (note how the bedding dip vectors may be fitted by a quadratic function) and have almost horizontal fold axes (Fig. 4). The dip and width of the common limb between the anticline and the syncline become gentler and smaller toward the ENE of the studied outcrop until the folds disappear (Fig. 3B).

The anticline-syncline pair is bounded to the north by a decameter- to hectometer-scale fault (Figs. 3 and 6). This fault is subvertical to steeply dipping to the S, and its strike is approximately E-W. No kinematic indicators were found on the fault surface, but it shows a reverse throw on the geological map (Fig. 3B), being the southern block (hanging wall) of the upthrown one. The fault orientation is slightly oblique to that of bedding in both the hanging wall and footwall and to that of the syncline-anticline pair described above (Fig. 3A). The limestones and marls of the Rodiles Formation exhibit a certain degree of brecciation in the fault zone. The fault displacement is around 36 m, estimated using the base of the Vega Formation as a reference bed. In the upthrown blocks of some neighboring faults, the Vega Formation rests unconformably on the underlying Rodiles Formation, the uppermost portion of which is missing (Suárez-Vega, 1974). This has been attributed to fault activity during the time in between the sedimentation of the uppermost Rodiles Formation and that of the lowermost overlying Vega Formation (Uzkeda et al., 2016). We ignored whether the displacement estimated for the fault described above, using the Vega Formation base as a reference bed, is the total value or a minimum value, which would be the case if the fault were active before sedimentation of the Vega Formation, similar to nearby faults.

Apart from the anticline-syncline pair and the reverse fault described above, the rocks are affected by several second-order structures; their types, dimensions, and numbers reflect a change in structural style up section in the hanging wall of the main reverse fault (Figs. 3C and 6C). In the lower part of the stratigraphic succession, where shales predominate, the density of structures is greater than in the upper part, where limestones predominate, but their dimensions are smaller. Second-order structures in the lower part consist mainly of thrusts and sporadic normal faults. The thrusts, which are the most numerous structures, are both NNW-directed and SSE-directed, exhibit ramp-flat geometry, and are up to 7–10 m length, and their maximum displacement is around 20–30 cm. The normal faults, usually NNW dipping and with small dimensions and displacement, seem to be cut and offset by the thrusts. In contrast, the upper part of the stratigraphic sequence is affected by fewer structures, and gentle fault-bend folds related to thrusts are the most common features. These thrusts form a SSE-directed imbricated system, display staircase geometries with ramps and flats, have a meter-scale length, and produce decimeter-scale displacements greater than those of the thrusts occurring in the lower part. This imbricated thrust system detaches at the upper part of a relatively thick, incompetent layer of dark marls that separates the upper and lower deformational domains (Fig. 7A). The cutoff angles between thrusts and bedding are usually 30° but, in some cases, may be as high as 60°. All

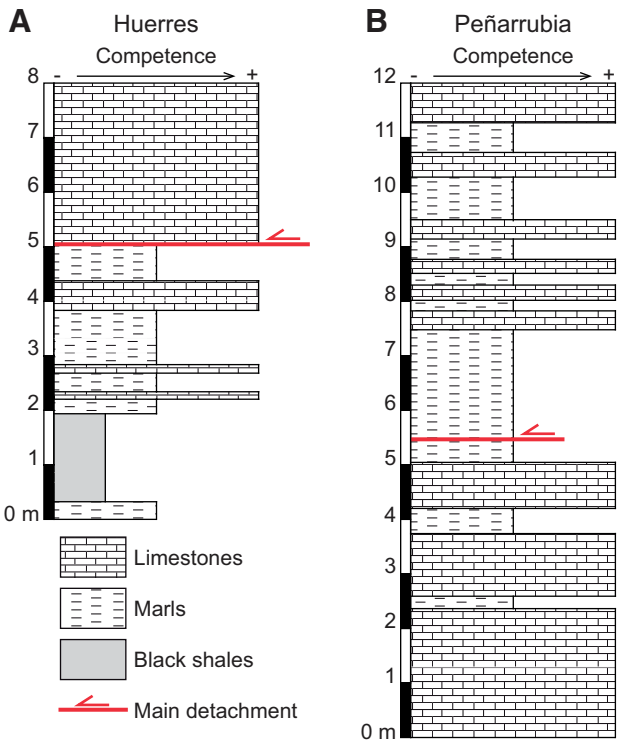

Figure 7. Mechanical-stratigraphic column of the (A) Huerres and (B) Peñarrubia outcrops.

the second-order contractional structures described here are restricted to the south block of the main reverse fault, i.e., its upthrown hanging wall, and do not appear in the fault footwall. They are concentrated in the area closest to the main fault and disappear southward away from the fault. In particular, they are concentrated in the forelimb of the main anticline. A few small-scale (not big enough to be mapped), NNE-dipping, right-lateral and NW-dipping, left-lateral faults also occur (Fig. 4D).

The structural relief of the Huerres main folds is ~2 m, measured using the most complete horizon in the geological cross section (turquoise blue horizon, third from bottom horizon in the cross section depicted in Fig. 6C), and taking the lowest point of the SSE syncline as a regional datum. Approximately 0.3 m (15%) of the structural relief was caused by minor thrust faults within the folds (estimated by adding the throw of the thrusts), whereas the rest was due to folding. To the structural relief value estimated, we must add 35 m due to the throw of the main reverse fault, which makes a total uplift of 37 m. Thus, more than 95% of the total uplift was due to faulting, whereas the rest was caused by folding. The shortening of the Huerres main folds is around 2 m (~10%), estimated by subtracting the width of the turquoise blue horizon in Fig. 6C from its total folded length. Approximately 1.3 m (60%) of the total shortening was produced by minor thrust faults within the main folds (estimated by adding the heave of the thrusts). In addition to the shortening value estimated, the main reverse fault has an approximate heave of 6 m, so that the total shortening is slightly above 8 m. Therefore, more than 90% of the total shortening was due to the contribution of faults, and the rest was due to folds. These data suggest that the Huerres structure was formed mainly due to faulting. This is in accordance with the geological maps of the surroundings of the studied outcrop, where faults are the predominant structures (Uzkeda, 2013; Uzkeda et al., 2016).

The layers located in the footwall of the main reverse fault dip to the N. In the hanging wall of the main fault, east and south of the studied outcrop, the layers also dip to the N (Fig. 3A). These observations point out a generalized layer tilting that involves both the hanging wall and footwall of the main reverse fault. The second-order folds and thrusts developed within the main anticline in the studied outcrop do not seem to have undergone this tilting, and, therefore, we assume that they developed after it.

Two almost-orthogonal families of joints were identified. The approximately N-S–striking family exhibits better-developed calcite fillings than the approximately E-W–striking family. Some of these fillings may contain traces of bitumen. The dips of both joint families range from 60° to 90°. Less-developed sets of joints occur, forming angles from 30° to 60° with the two main families. The temporal relationships between the joints and folds and faults are unclear.

The black shales rich in organic matter located in the lower part of the stratigraphic succession contain several centimeter- to decimeter-length veins filled with carbonate, iron sulfides, and iron oxides, as well as other components. These veins are folded by a large number of millimeter- to centimeter-scale, recumbent folds (Fig. 8). The axial surfaces of these recumbent folds are approximately parallel to bedding surfaces, so that bedding surfaces are not folded. This suggests that the principal compressive stress responsible for vein folding was perpendicular to bedding. These veins may have formed during compaction of the shales as a result of fluid expulsion and precipitation of carbonate and iron-rich minerals. An alternative explanation is that they were caused by tectonic layer-parallel shear; however, the lack of a consistent fold asymmetry leads us to discard this hypothesis.

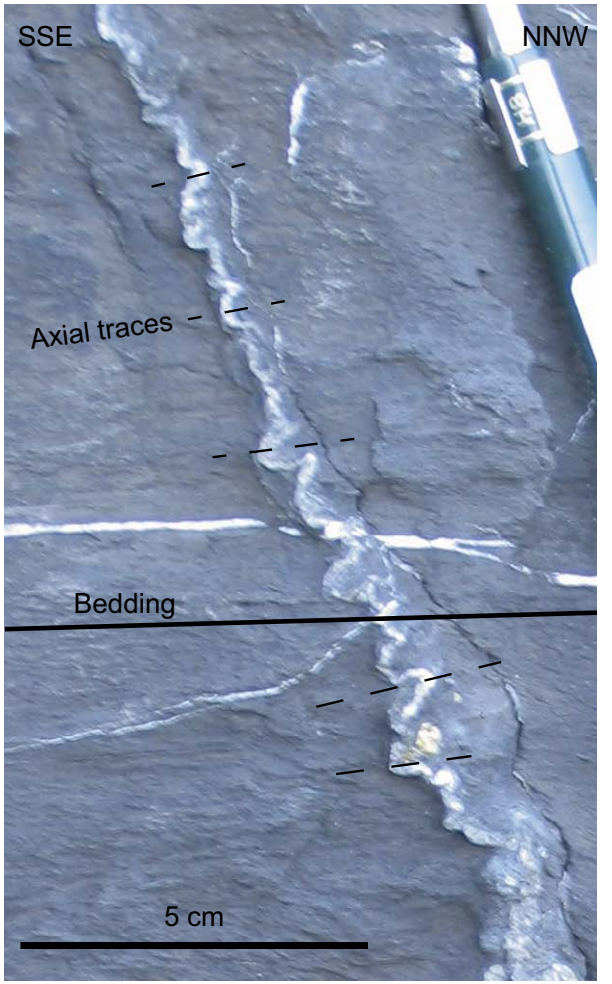

Figure 8. Veins folded by millimeter- to centimeter-scale recumbent folds for which the axial planes are approximately parallel to bedding.

To the NE of the studied outcrop, a few map-scale, apparently strike-slip faults occur (Fig. 3B). The most important fault is the one closest to the mapped structure; it is a NW-SE subvertical fault of decametric dimensions that causes a strike separation of around 4 m in the sandstone beds located at the base of the Vega Formation. Unfortunately, no kinematic indicators associated with this fault were observed, but the fault motion deduced from correlation of homologous layers in both fault blocks suggests a left-lateral fault, a fault in which its northeast block would be the downthrown block, or an oblique fault involving both motion components. This fault offsets the main reverse fault in the geological map depicted in Figure 3B; however, this temporal relationship is unclear, since the fault intersection area is partially covered by rocks fallen from the coastal cliff. The major folds described above disappear in the area where these two faults intersect.

Kinematic Evolution

We interpreted the Huerres structure in terms of inversion tectonics because of the following reasons.

(1) Small-scale normal faults that developed prior to thrust faults were identified in the outcrop (Fig. 3C), indicating that there was an extensional event followed by a contractional event.

(2) The obliquity between the main anticline-syncline pair and the main reverse fault (Fig. 3B) may support the existence of structures formed under different stress fields, as proposed by Uzkeda (2013) and Uzkeda et al. (2016), and, therefore, the existence of inversion tectonics.

(3) The fact that the contractional structures (main folds and related second-order thrusts) are restricted to a portion of the main fault hanging wall and disappear when moving farther away from the fault, and the fact that the main fault footwall was not affected by contractional structures suggest that the main fault footwall may have played a buttressing role. Buttressing as a result of a compressive event affecting preexisting normal faults has been documented in neighboring faults (Martín et al., 2013; Uzkeda et al., 2013). The incompetent thick succession in the fault hanging wall relative to more competent footwall rocks, together with the elevated dip of the main normal fault, supports the buttressing hypothesis. The vergence of the principal anticline opposite to the main fault dip, and thrusts directed opposite to the main fault dip also support the buttressing hypothesis. Thus, the effect exerted by the main fault footwall could be compared, to a certain extent, to that exerted by backstops in many laboratory physical experiments where the structures verge and are directed toward the opposite sense.

The anticline-syncline pair located in the hanging wall of the main reverse fault might be interpreted as detachment folds. The occurrence of incompetent, thick black shales in the core of the anticline may support this hypothesis. If this were true, the spatial variations in fold geometry may be used to decipher the fold temporal evolution following the method proposed by Poblet et al. (1998). Thus, the decreasing dip and width of the common limb between the anticline and syncline toward the fold termination (Figs. 3B and 9) suggest that the fold amplification mechanism that operated was a mixture of limb rotation and hinge migration. Such a combination of mechanisms has been proposed for theoretical models of detachment folds (e.g., Poblet and McClay, 1996), as well as for surface and subsurface folds in different regions (e.g., Poblet et al., 2004).

Figure 10 illustrates schematically a possible evolution of the Huerres structure from its initiation to present day. An approximately E-W normal fault subperpendicular to bedding developed during the extensional period. This fault was located within a large rollover related to a major fault to the north of the studied outcrop. Strong inversion tectonics, fundamentally due to faulting, took place during a subsequent contractional event, and the normal fault underwent reverse reactivation with a dextral component accompanied by a buttressing effect in the fault hanging wall. Buttressing was responsible for a detachment anticline adjacent to the normal fault with vergence opposite to the sense of motion of the reactivated normal fault. The anticline forelimb amplified by rotating and lengthening. Synchronously, a detachment, directed in the opposite sense to that of the reverse reactivation of the normal fault, developed in the main fault hanging wall. This detachment separates the lower incompetent from the upper competent hanging-wall packages with second-order structures of different types, dimensions, and abundance. The buttressing effect was triggered when the reverse reactivation of the inherited normal fault brought into contact rocks of different competence in the fault hanging wall and footwall, which, together with the steep fault dip, prevented contractional deformation from propagating toward the main normal fault footwall. Thus, the inherited normal fault exerted a strong control on the type and distribution of contractional structures in the fault hanging wall (Figs. 3B and 6). The extensional structures are assumed to be a Jurassic and/or Cretaceous feature, whereas the inversion tectonics occurred during Cenozoic times, similar

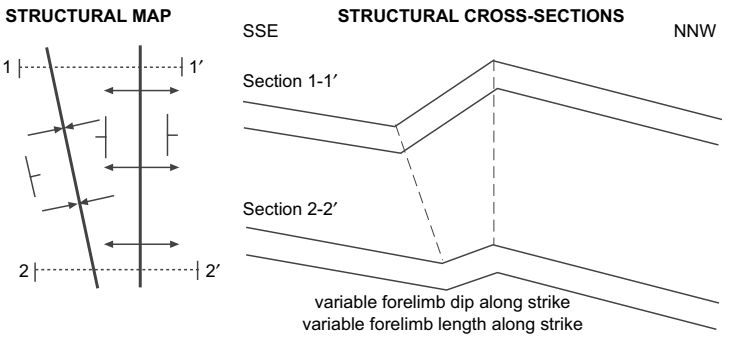

Figure 9. Schematic structural map and cross sections showing the along-strike variation of dip and width of the common limb between the major anticline and syncline for the Huerres structure. Both decrease toward the eastern termination of the structure.

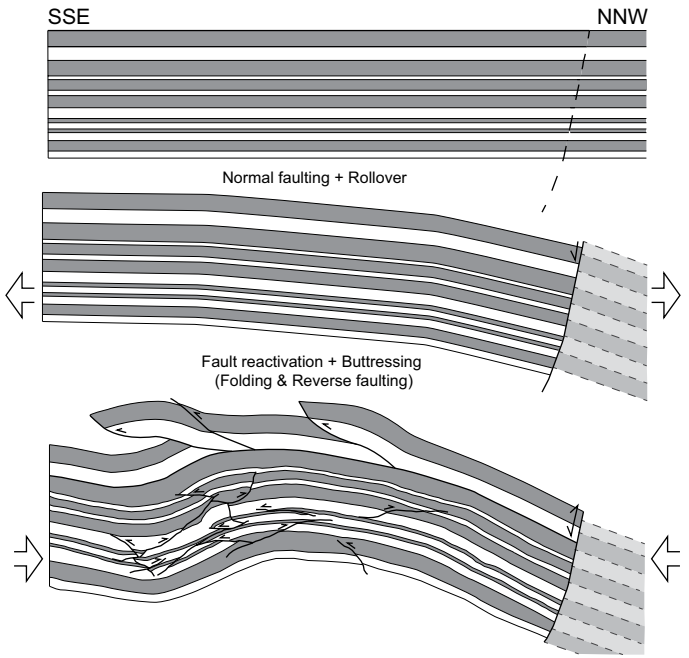

Figure 10. Schematic cartoon showing possible structural evolution of the Huerres structure from the undeformed state to present day.

to other structures documented in nearby regions within the Asturian Basin (Lepvrier and Martínez-García, 1990; Uzkeda et al., 2016; amongst others).

The effects of the contractional deformation seem to decrease along strike toward the eastern portion of the main fault hanging wall, where the folds disappear (Fig. 3B). Alternatively, the shortening could have remained approximately constant along strike, whereas to the west, it would have been accommodated by reverse displacement along the main fault plus folding, and toward the east, it would have been accommodated solely by reverse displacement along the main fault. To the east of the study area, the cutoff lines between the horizons and the fault exhibit a certain dip component toward the W, and, therefore, the reverse displacement of the fault would increase eastward. This would support the second hypothesis.

PEÑARRUBIA STRUCTURE

The Peñarrubia structure is located in the west portion of the Peñarrubia Beach, in the east part of Gijón (Figs. 1A and 1C). The studied structure crops out along an approximately E-W coastal cliff, around 25 m wide and 10 m high. The studied outcrop shows irregularities, with faces at different depths and approximately flat areas that usually correspond to bedding surfaces. After the initial conventional geological tasks, such as geological mapping (Fig. 11A), photogeological interpretation of conventional photographs (Fig. 11B), and structural data analysis (Fig. 12), 63 high-dynamic-range photographs were shot from different points of view to cover the whole outcrop (Fig. 13A). Subsequently, six control and 18 check points distributed along the outcrop were taken to georeference and check the quality of the point cloud, respectively (Fig. 13B). The point cloud was interpreted from the geological point of view (Fig. 14A). The 3-D geological data obtained, together with dips and strikes of beds and faults plus the plunge of fold axes, allowed us to construct bedding and fault surfaces (Fig. 14B). Finally, a cross section approximately perpendicular to the fold axes was derived from the 3-D geological model (Fig. 14C). A comparison of the coordinates of the check points measured in the point cloud and those measured in the field yielded an average quadratic error of 2.9 cm. Moreover, 10 measurements of strike and dip of stratification surfaces were taken in different locations of the point cloud and compared to data taken in the field at the same position. The angular differences between both sets of measurements ranged between 4° and 15°, being the average close to 11°. The difference between the coordinates of the check points and the orientation of bedding surfaces measured in the point cloud and those measured in the field is relatively small given the errors arising from the irregularity of the stratification surfaces and the measuring instruments, as well as errors when taking the measurements and interpreting the data. Therefore, this suggests that the point cloud constructed is quite accurate and allows us to obtain quantitative geological data from its analysis.

Structural Features

The Peñarrubia structure consists of a decameter-scale anticline-syncline pair. They are approximately parallel, open folds (Figs. 11, 13B, and 14) with an interlimb angle less than 120° (Fig. 12). The structural relief measured in the anticline is around 1.5 m. These folds verge toward the W; the axial surfaces strike N-S and dip moderately to the E, whereas the fold axes are slightly curved and dip from gently to the N to horizontal to gently to the S. The anticline has a long, NW-SE–striking east limb (backlimb) gently dipping to the NE and a short, N-S–striking west limb (forelimb), common to the syncline, moderately dipping to the W. The west limb of the syncline is subhorizontal. The fold traces on the map are slightly curved, approximately N-S to the south, and NNW-SSE toward the north (Fig. 11A). These folds are cylindrical, as both the equal-area projections and the tangent diagrams suggest (Fig. 12).

Three major, meter- to decameter-length faults occur in between the anticline and syncline hinge zones (Figs. 11B and 14). These faults strike N-S and dip moderately to the E, are oblique to bedding almost everywhere, and cause centimeter to decimeter displacements. The easternmost and westernmost faults are reverse, whereas the fault in between them is normal and displays

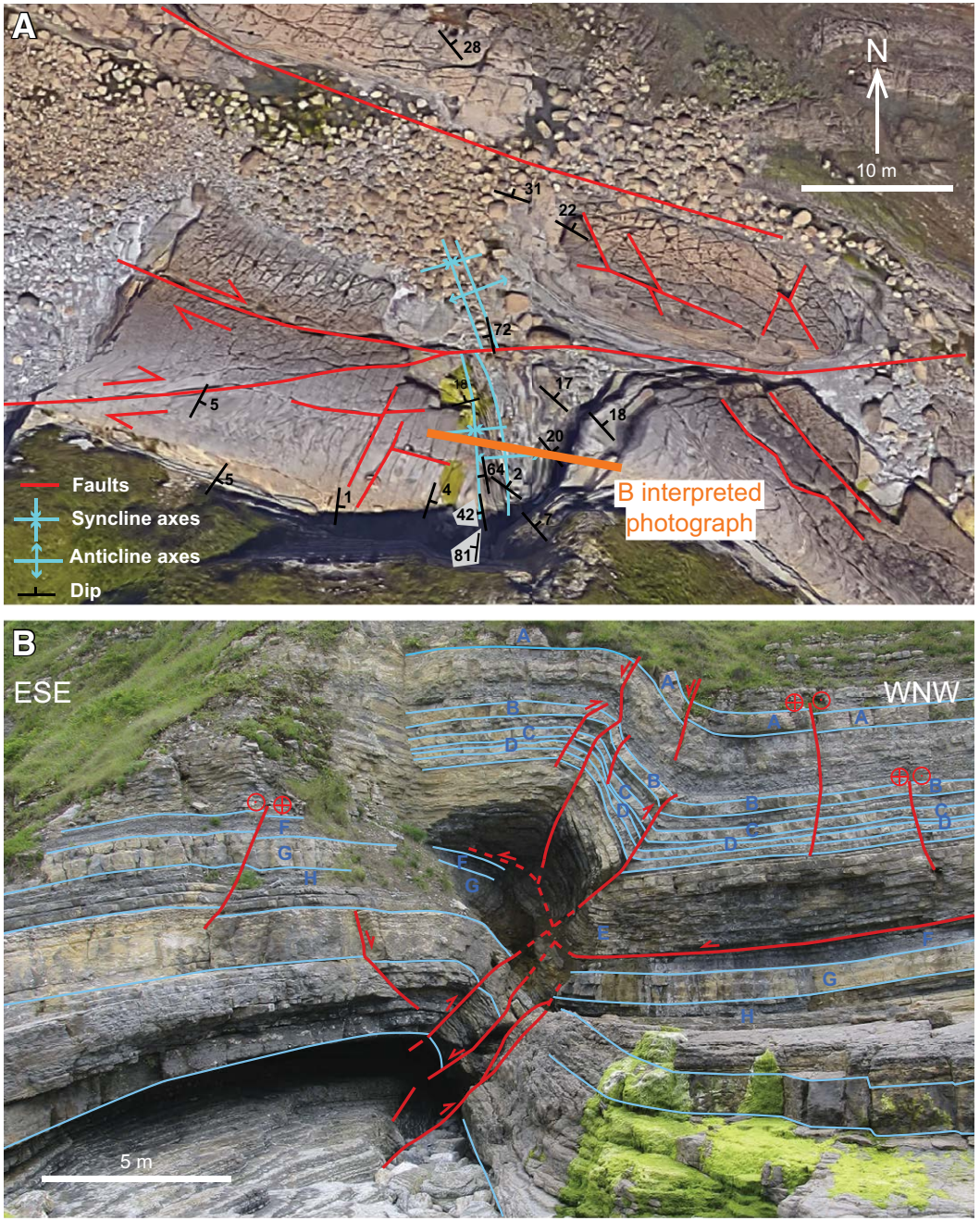

Figure 11. (A) Geological map of the Peñarrubia outcrop and surrounding areas on top of a 2016 Google Earth photograph with location of the photograph illustrated in B. See Figure 1 for location of this map within the Asturian Basin. (B) Photograph of the Peñarrubia outcrop along with its geological interpretation. The structure involves alternations of gray limestones and marls (Buerres Member, Rodiles Formation). Limestones predominate in the lower part of the outcrop, whereas alternations of limestones and marls predominate in the upper part (beds A to H). Blue lines—bedding, red lines—faults.

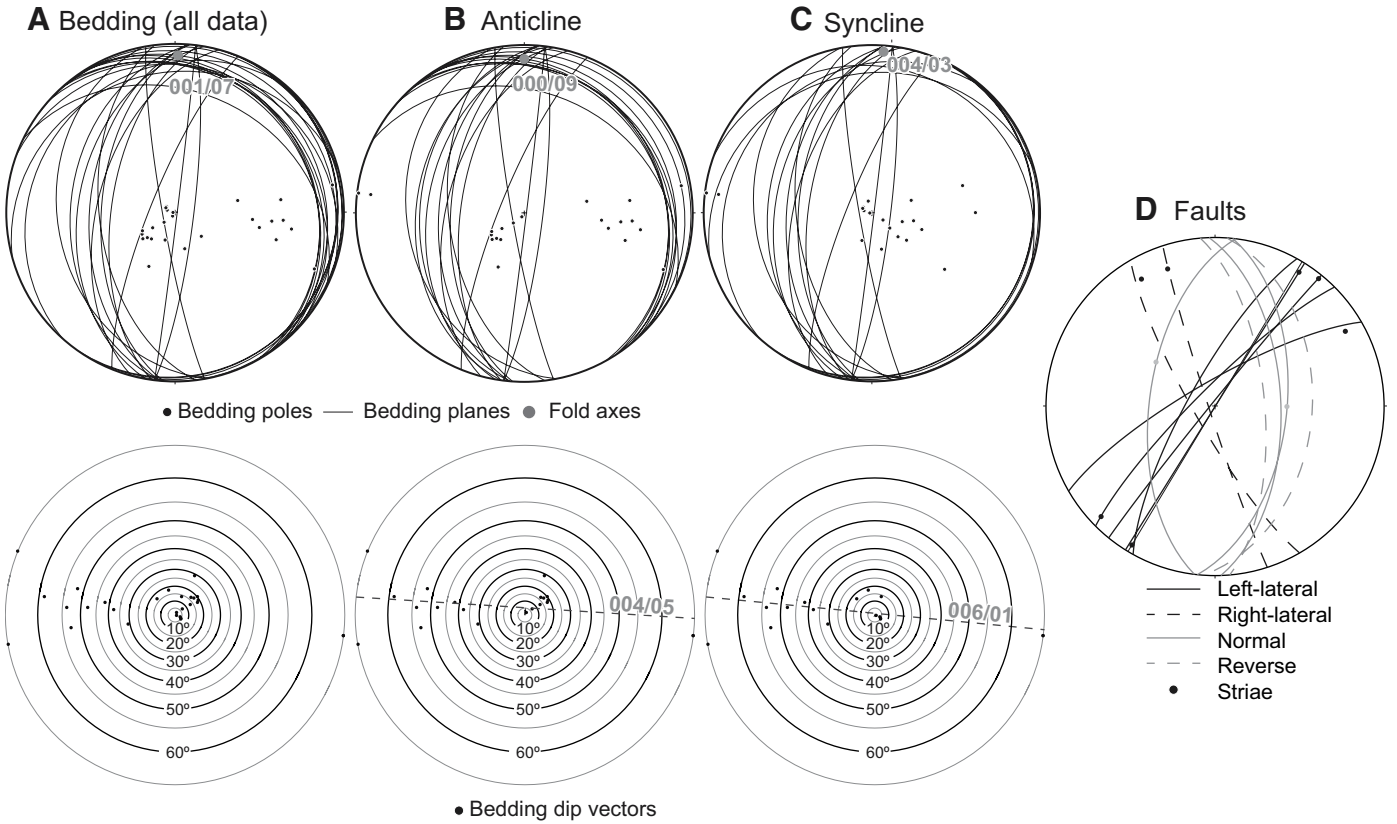

Figure 12. Equal-area projections in the lower hemisphere and tangent diagrams of orientation data collected in the Peñarrubia outcrop. (A) Bedding (surfaces and poles); (B) bedding (surfaces and poles) and average fold axis for the anticline; (C) bedding (surfaces and poles) and average fold axis for the syncline; and (D) faults, along with their kinematic indicators. Equal-area projections were plotted using the software Stereonet. Tangent diagrams have 5° increments. The bedding dip vectors displayed in the tangent diagrams have been fitted using a linear function.

almost dip-slip kinematic indicators (striae). Some of these faults are located in different structural positions, offsetting the stratigraphic succession involved in this structure, the lower part of which is more competent and consists of gray limestones and a small amount of intercalated gray marls, and the upper part of which is less competent and is made up of alternations of gray marls and limestones. The easternmost reverse fault breaks through the anticline hinge in the lower part of the succession and runs through the syncline hinge in the upper part of the succession. The westernmost reverse fault runs through the anticline forelimb in the lower part of the succession and dies out at a syncline hinge in between the two successions. The normal fault in between the reverse faults runs through the anticline forelimb in the lower part of the succession and through the anticline hinge in the upper part of the succession. A detachment, located at the top of a marly level, separates the more competent (below) from the more incompetent (above) parts of the succession (Fig. 7B). This detachment involves ESE-directed motion and has ~2 m of displacement; the detachment offsets a subvertical normal fault, approximately perpendicular to the detachment surface, toward the west of the studied outcrop. This detachment is folded by the anticline-syncline pair and cuts and offsets the normal fault, and it is cut and offset by the easternmost reverse fault.

The structural relief of the Peñarrubia structure is 1.4 m, measured using the most complete horizon in the geological cross section (dark-green horizon, eighth horizon beginning from the bottom horizon in the geological cross section depicted in Fig. 14C) and taking as a regional datum the lowest point of the syncline to the west of the anticline. Approximately 0.1 m (7.1%) of the

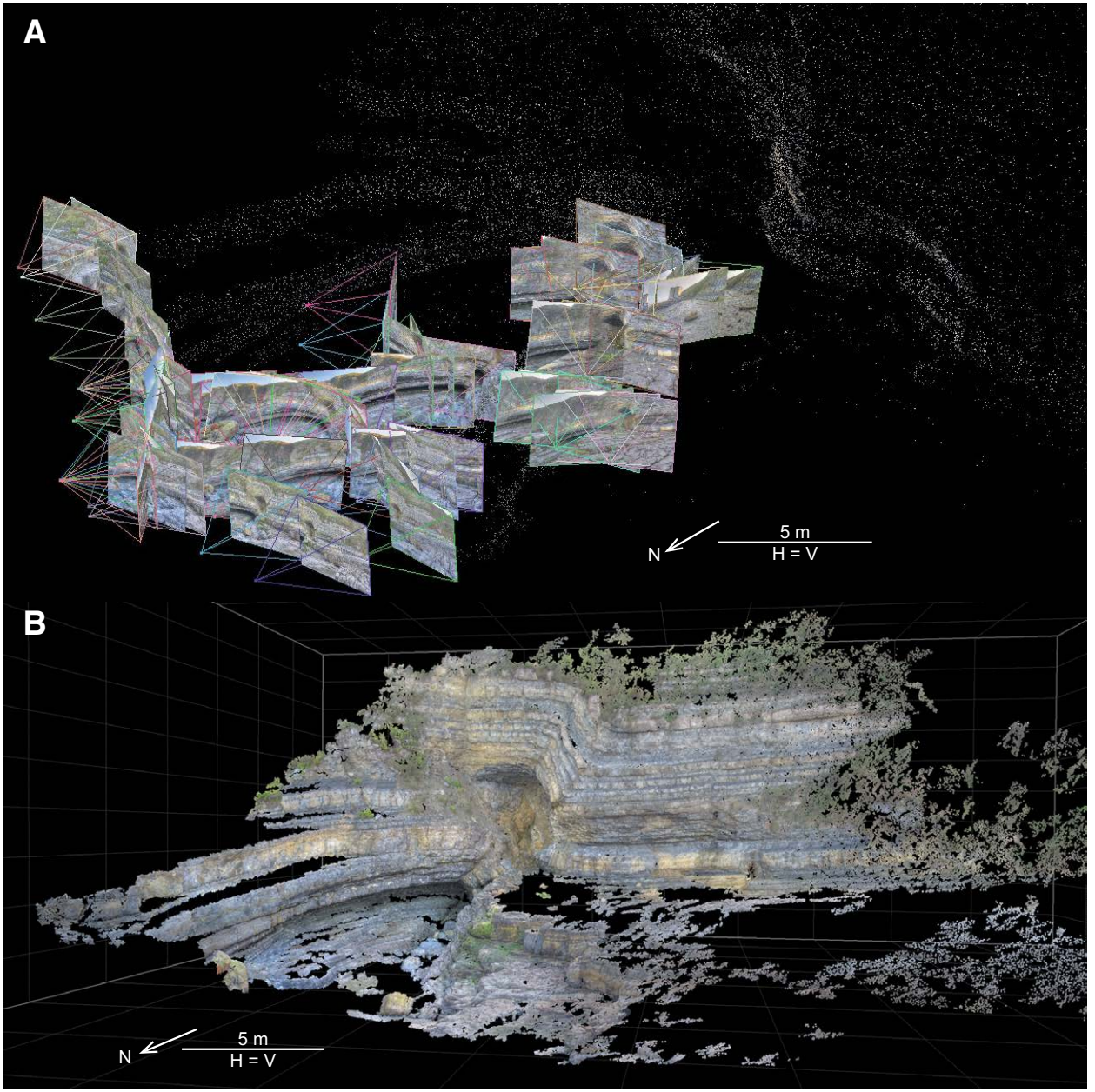

Figure 13. (A) High-dynamic-range photographs employed to construct the virtual outcrop model of the Peñarrubia outcrop in the form of a point cloud, displayed in (B). The software VisualSFM was used to construct the point cloud. H—horizontal, V—vertical.

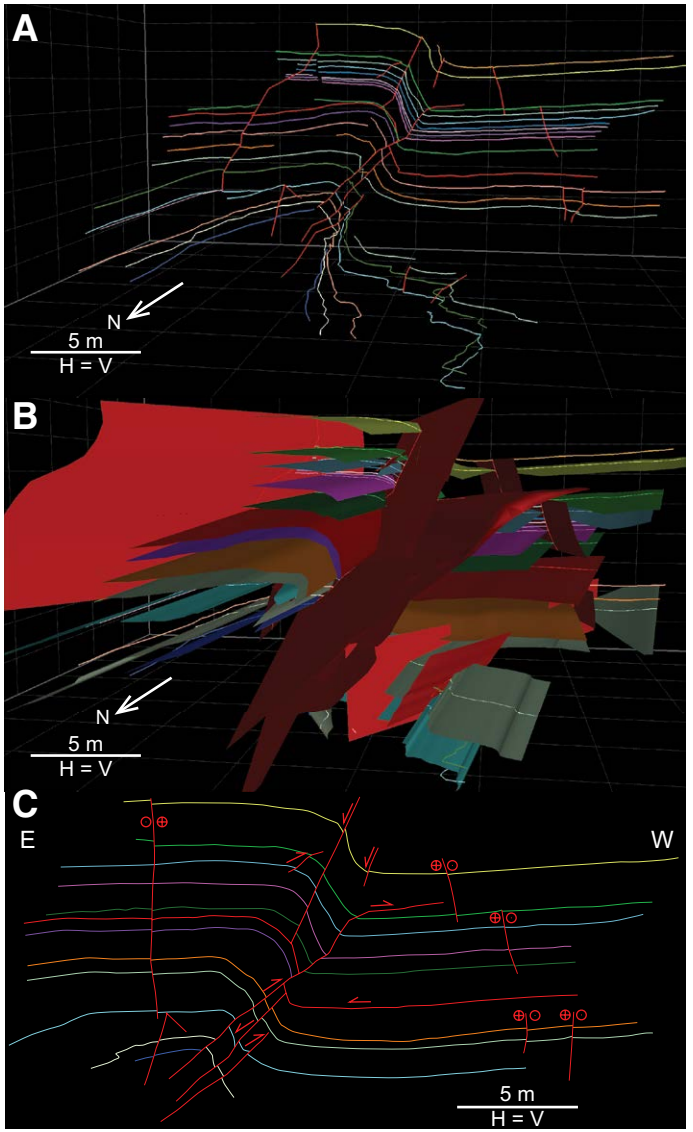

Figure 14. (A) Three-dimensional (3-D) geological interpretation of the Peñarrubia point cloud displayed in Figure 13B carried out with the software 3-D Stereo VDT in a computer-assisted virtual environment (CAVE). (B) 3-D geological model of the Peñarrubia outcrop constructed using the software Move, field data, and the CAVE interpretation shown in A. (C) Geological section across the Huerres structure obtained from the 3-D geological model displayed in B. Red lines and surfaces—faults, other color lines and surfaces—bedding, H—horizontal, V—vertical.

structural relief is due to faulting (estimated by adding the throw of the reverse faults), while the rest is due to folding. We obtained a shortening amount of 1 m (7.9%) by comparing the folded length of the dark-green horizon with its width. Thereby, 0.1 m (10% of the total shortening) was due to faulting (estimated by adding the heave of the reverse faults), and the rest was due to folding. The measured uplift and shortening values indicate that the Peñarrubia structure was mainly caused by folding (Figs. 11 and 14). This is in accordance with the geological maps of the area surrounding the studied outcrop, where folds are the most common structures (Odriozola, 2016).

A few second order, meter-scale, strike-slip faults were identified (Fig. 10D). They usually consist of NW-SE right-lateral faults and NE-SW left-lateral faults. All of them exhibit steep dips, usually greater than 80°; the right-lateral faults dip toward the SW, and the left-lateral faults dip toward the NW. Most of them have subhorizontal kinematic indicators such as striae. In cross-sectional view, these faults produce small throws that may reach 10–20 cm and may appear to be reverse or normal depending on the pitch of their kinematic indicators. The northwestern fault block of many NE-SW left-lateral faults corresponds to the downthrown block. Some right-lateral faults cut and offset left-lateral ones; however, in some outcrops, both families seem to be synchronous and are probably conjugate faults.

In addition, a decameter-scale, right-lateral fault with an approximately E-W strike and steep dip offsets the Peñarrubia structure around 3 m (Fig. 10A) and is responsible for a small drag fold in the vicinity of the fault.

Kinematic Evolution

Apparently, the Peñarrubia structure displays the typical geometry of a pure contractional structure. However, some elements, listed below, suggest that a previous extensional event took place.

(1) Both normal and reverse faults have been mapped in the studied outcrop (Figs. 11B and 14), which could indicate at least two tectonic episodes, an extensional one and a contractional one.

(2) The detachment located in between the upper and lower stratigraphic successions cuts and offsets a normal fault, subperpendicular to bedding, in the forelimb of the anticline (Figs. 7B, 11B, and 14). Assuming that the detachment is the oldest contractional feature in this outcrop, this suggests the occurrence of an extensional event followed by a contractional one.

The most noticeable structural features of the Peñarrubia outcrop, i.e., a parallel anticline developed in the hanging wall of a thrust (westernmost reverse fault) that dies out at the hinge of the frontal syncline, indicating that its displacement decreases up section toward its termination, suggests that this structure could be interpreted as a fault-propagation fold (Suppe and Medwedeff, 1990). Assuming that serial geological sections across the termination of a fold reflect its temporal evolution, then the constant dip and decrease of width of the common limb between the anticline and the syncline along strike as we approach the fold termination to the north (Figs. 10A and

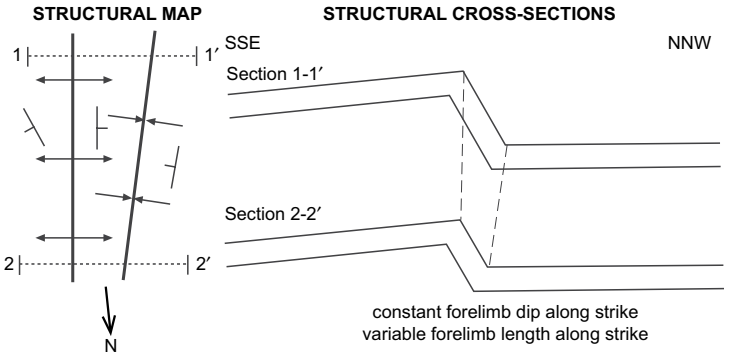

Figure 15. Schematic structural map and cross sections showing the along-strike variation of dip of the common limb between the major anticline and syncline for the Peñarrubia structure. It decreases toward the northern termination of the structure.

15) indicate, according to Poblet et al. (1998), that the anticline forelimb was amplified through the hinge-migration mechanism. Anticline forelimb hinge-migration is also consistent with the interpretation of this structure as a fault-propagation fold. The main difference between the Peñarrubia structure and most fault-propagation folds documented in the literature is that the thrust responsible for the Peñarrubia structure is oblique to the anticline backlimb. This situation has been documented in some types of fault-propagation folds such as trishear fault-propagation folds (Erslev, 1991), double-edge fault-propagation folds (Uzkeda et al., 2010), etc. The easternmost thrust running from the anticline hinge to the syncline hinge up section, cutting through the anticline forelimb, is interpreted as a breakthrough thrust.

Figure 16 illustrates schematically a possible evolution of the structure from its initiation to present day. Initially, during the extensional episode, the Peñarrubia structure was a small-displacement normal fault subperpendicular to bedding. During the contractional episode, a SE-directed detachment cut and offset the normal fault. This detachment separates a more competent, lower package from a less competent, upper package. Subsequently, a fault-propagation fold started to develop with a vergence opposite to that of the detachment sense of displacement. The anticline forelimb increased its width while maintaining its initial dip, while the main thrust propagated toward the core of the frontal syncline. At a certain stage of fold development, a breakthrough thrust cut and offset the anticline forelimb, involving almost all the stratigraphic succession. As a result, the detachment was folded by the fault-propagation fold and offset by the breakthrough thrust. Thus, the old extensional structure underwent inversion tectonics due to a contractional event. Finally the whole structure was cut and offset by a dextral, approximately E-W, steep fault. The homogeneous nature of the rocks in the hanging wall and footwall of the Peñarrubia main normal fault and the relatively small displacement of the normal fault indicate that the geometry of the layers just before the

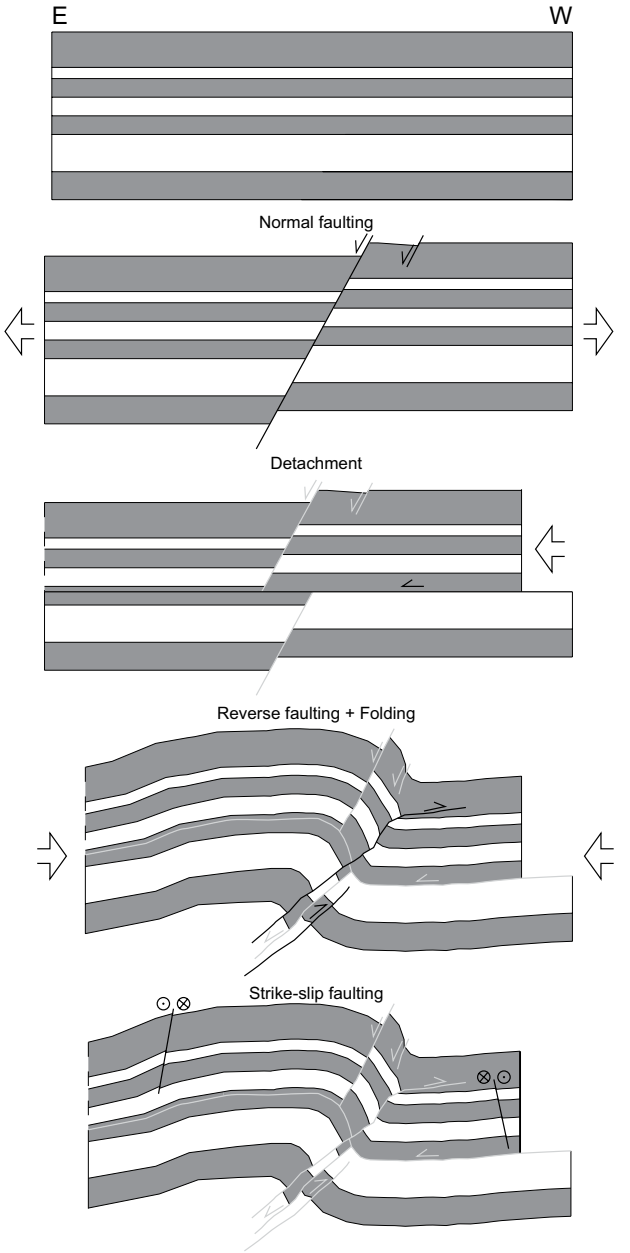

Figure 16. Schematic cartoon showing the possible structural evolution of the Peñarrubia structure from the undeformed state to present day.

contractional episode was mostly undeformed; this may be the reason why the inversion tectonics gave rise to an almost typical contractional structure, where almost no record of the inherited extensional structure is preserved. The main control exerted by the normal fault consisted of the initial perturbation, where the fault-propagation fold developed and conditioned the position of the anticline axial surface in the upper part of the stratigraphic succession (Figs. 11B and 14). As in other structures within the Asturian Basin, we assume that the extensional event took place sometime during the Jurassic and/or Cretaceous, and the contractional inversion tectonics occurred during Cenozoic time (e.g., Lepvrier and Martínez-García, 1990; Uzkeda et al., 2016).

COMPARISON BETWEEN THE HUERRES AND PEÑARRUBIA STRUCTURES

We have recognized important coincidences and differences between the Huerres and Peñarrubia structures in terms of the stratigraphic succession involved in the structures and the structures themselves (Table 1). Thus, both structures involve alternations of limestones and marls of Early to Middle Jurassic age; they display variations in the structural style of the contractional structures up section, because they consist of two stratigraphic packages of different competence separated by a folded detachment; the scale of both structures is similar; the nucleation of the contractional structures was conditioned by the existence of a previous normal fault; the second-order contractional faults are concentrated in the forelimb of the main anticlines; and they underwent a similar degree of inversion tectonics.

The most important differences between both outcrops concern the contractional episode responsible for inversion tectonics. Thus, the Huerres structure is interpreted as undergoing oblique-reverse reactivation of an original normal fault accompanied by buttressing in its hanging wall. This would have caused detachment folding, decoupling of an upper and a lower structural level, and second-order thrusting. On the contrary, the Peñarrubia structure is interpreted as a thrust-propagation fold involving a forelimb breakthrough thrust. The thrust-propagation fold was responsible for folding and offsetting a detachment, which in turn offset the old normal fault. In the Huerres outcrop, all the contractional structures are interpreted to have been active at approximately the same time, i.e., the reactivation of the normal fault and the folding. On the contrary, in the Peñarrubia outcrop, activity of the contractional structures was not simultaneous, so that the detachment was the first one to develop, followed by the fault-propagation fold. In the Huerres outcrop, the position, sense of motion, and vergence of the main contractional structural elements simulate a sort of "pop-up" structure; thus, the main fault, located to the north, is N-directed, whereas the folds, located to the south, are S-vergent. However, in the Peñarrubia outcrop, the position, sense of motion, and vergence of the structures resembles a sort of "triangular zone," because the E-directed detachment moved toward the W-vergent fault-propagation fold. In the Huerres outcrop, the inversion tectonic structures developed in the normal fault hanging wall, whereas in the Peñarrubia outcrop, the structures developed in both the hanging wall and footwall of the normal fault.

In both outcrops, the inversion tectonics and the kinematic evolution during the contractional event were strongly influenced by rheological parameters, as well as by the main geometrical features of previous extensional structures and their orientation in relation to the contractional stress field. The mechanical stratigraphy of the rocks involved in the structures turned out to be one of the main parameters that controlled the type, dimensions, number, and distribution of contractional structures.

CONCLUSIONS

The main features of the meter- to decameter-scale outcrops studied here suggest that a wide range of different types of tectonic inversion structures, resulting from Mesozoic extensional faults subjected to a Cenozoic contractional event, may coexist in the Asturian Basin:

(1) from faulting-dominated to folding-dominated inversion tectonics;

(2) from inversion tectonics structures reusing inherited normal faults (reverse and/or strike-slip fault reactivation) to other types of interaction between old normal faults and inversion tectonics structures (normal faults cut, offset, and/or folded by newly generated contractional structures);

(3) from inversion tectonics structures consisting of detachment fold types to fault-propagation fold types;

(4) from inversion tectonics structures with divergent senses of motion, similar to a certain extent to "pop-ups," to inversion tectonics involving convergent senses of motion, similar to "pseudo-triangular zones";

(5) from inversion tectonics structures restricted to the inherited normal fault hanging wall to inversion tectonics structures developed in both the fault hanging wall and footwall, highly dependent on the mechanical contrast of both fault blocks; and

(6) from inversion tectonics structures where the type, main features, and distribution were strongly controlled by the inherited normal faults to inversion tectonics where the only control by the inherited normal faults was the locus at which they developed.

The use of virtual outcrop models was essential to this research. Without them, it would have been virtually impossible to obtain geological cross sections that properly illustrated the correct geometry of the structures. Geological cross sections derived from conventional photogeological interpretation and from traditional cross-section construction in the field exhibited large distortions due to the irregularity of the outcrops. In addition, the irregular shape of the outcrops made it difficult to correlate the different layers from one end to the other end of the outcrops, especially because the outcrops are made up of relatively thin alternating layers of two predominant lithologies. The analysis presented herein was facilitated by the use of virtual outcrop models. In addition, the resulting models provided a fast and easy way to measure fault

TABLE 1. COMPARISON BETWEEN HUERRES AND PEÑARRUBIA STRUCTURES

	HUERRES	PEÑARRUBIA
Stratigraphy and mechanical stratigraphy		
Formation	Rodiles	Rodiles
Member	Santa Mera	Buerres
Age	Lower–Middle Jurassic	Lower Jurassic
Incompetent package	Black shales, limestones	Gray marls, limestones
Competent package	Gray limestones, marls	Gray limestones, marls
Stratigraphic position of incompetent rocks	Bottom	Top
Structural position of incompetent rocks	Hanging wall of the main normal fault	Hanging wall and footwall of the main normal fault
Mechanical contrast between hanging wall and footwall	High	Low
Broad structure		
Scale	Decameter	Meter-decameter
Strike	Approximately E-W	Approximately N-S
Extensional structure		
Main normal fault dip	Subvertical (subperpendicular to bedding)	Moderate to the E (subperpendicular to bedding)
Main normal fault displacement	Decameter (reverse)	Centimeter to decimeter (normal)
Contractional structure		
Variation of structural style up section	Important (type, size, number, and distribution of second-order structures)	Subtle (position and number of main faults)
Structure separating structural styles	Folded detachment (decimeter to meter slip)	Folded detachment (decimeter to meter slip)
Detachment timing	Coeval to the rest of contractional structures	Oldest contractional structure
Detachment sense of displacement	Equal to the vergence of the main contractional structures (SSW)	Opposite to the vergence of the main contractional structures (E)
Upper structural style	Few, large fault-bend folds and related thrusts (imbricated system)	Two main faults along fold hinges
Lower structural style	Fewer, small thrusts	Three main faults within main anticline forelimb
Main fold vergence	SSE (same as main normal fault dip)	W (opposite to main fault dip)
Main fold interlimb angle	Gentle to open	Open
Main fold amplification mechanism	Limb rotation + hinge migration	Hinge migration
Distribution of folds and faults	Restricted to the main normal fault hanging wall	Developed in both blocks of the main normal fault
Concentration of second-order faults	Main fold forelimb	Main fold forelimb
Structure uplift	37.1 m (95% fault and 5% fold)	1.4 m (7% fault and 93% fold)
Structure shortening	8.3 m (90% fault and 10% fold)	1 m (10% fault and 90% fold)
Inversion tectonics		
Normal fault reactivation	Important reverse fault with dextral component?	No apparent reactivation
Contractional structures offsetting main normal fault	None	Detachment
Main inversion tectonics mode and kinematic evolution	Normal faulting + tilting, reverse (dextral) fault reactivation + buttressing (detachment folds, second-order thrusts and detachment)	Normal faulting, detachment, fault-propagation fold involving a forelimb breakthrough thrust
Inversion tectonics degree	Strong	Strong
Principal influence of the main normal fault	Type and distribution of contractional structures	Position of the axial surface of the main contractional fold
Late dextral faults	Possible	Yes

displacements and to obtain orientation data from elements of interest, which was particularly handy in those areas not accessible in the field, e.g., upper parts of the outcrops.

The structural interpretation of the outcrops carried out here may provide assistance in the geological interpretation of particular structures imaged in the seismic data of the offshore portion of the Asturian Basin. This should help to improve the models used to date in order to explore for hydrocarbons (Riaza Molina, 1996). Furthermore, it should also be of assistance for the accurate geological mapping of less well-exposed onshore areas of the basin away from the coast, where substantial vegetation cover occurs. In addition, it may contribute to a better understanding of the deep structure of the Asturian Basin, which is very important for the comprehension of the formation and structuring of this part of the North Iberian margin. It may also have consequences on the selection of possible sites for placing state reserve acreage for CO_2 storage, since this region has been chosen, together with adjacent ones, as an area of potential interest. Finally, the structural interpretations carried out here may serve as analogues for structures developed in similar extensional regions that have undergone inversion tectonics.

ACKNOWLEDGMENTS

Comments and suggestions by Editors Raymond M. Russo and Francesco Mazzarini, and the reviewers Richard Groshong and Ken McCaffrey substantially improved the manuscript. We would like to acknowledge financial support by the research project CGL2015–66997-R: "Aplicación del análisis del plegamiento a la investigación de recursos geológicos" (AAPLIREGE) funded by the Spanish Ministry for Economy and Competitiveness and the European Fund for Regional Development (FEDER) and research contract CN-16–014: "Convenio específico para la realización de un trabajo de investigación post-doctoral en la disciplina de Geología" under the framework agreement between Repsol Exploración S.A. and the University of Oviedo. We thank Changchang Wu for permission to use the software VisualSFM, the Visual Computing Lab-ISTI-CNR for permission to use MeshLab, Midland Valley for permission to use Move (Academic site software license and support agreement number 1915), and Richard Allmendinger and Nestor Cardozo for permission to use Stereonet. We thank J.L. Alonso, J.C. García-Ramos, and L. Piñuela for helping us with structural and stratigraphic issues, M. Odriozola for assisting us during field campaigns, I. Moriano for her tests of the initial versions of the 3-D Stereo VDT software, J.G. Antuña and I. Sobrado for maintaining the software for structural interpretation and modeling, and J.M. González Cortina for preparing the global positioning system (GPS) equipment.

REFERENCES CITED

Alonso, J.L., and Pulgar, J., 2004, Estructura alpina de la Cordillera Cantábrica: Generalidades, *in* Vera, J.A., ed., Geología de España: Madrid, Spain, Instituto Geológico y Minero de España, p. 332–334.

Alonso, J.L., Pulgar, J., García-Ramos, J., and Barba, P., 1996, Tertiary basins and Alpine tectonics in the Cantabrian Mountains (NW Spain), *in* Friend, P.F., and Dabrio, C.J., eds., Tertiary Basins of Spain: The Stratigraphic Record of Crustal Kinematics: New York, Cambridge University Press, p. 214–227, https://doi.org/10.1017/CBO9780511524851.031.

Alonso, J.L., Gallastegui, J., Garcia-Ramos, J.C., and Poblet, J., 2009, Estructuras Mesozoicas y Cenozoicas Relacionadas con la Apertura y Cierre Parcial del Golfo de Vizcaya (Zona Cantábrica–Asturias): 6th Simposio Sobre el Margen Ibérico Atlántico (MIA), Field Trip Guidebook: Oviedo, Spain, 18 p.

Alonso, M., 2014, Análisis Estructural de los Materiales Jurásicos de la Playa de El Rinconín, Gijón [M.Sc. thesis]: Oviedo, Spain, Universidad de Oviedo, 47 p.

Bádenas, B., Armendáriz, M., Rosales, I., Aurell, M., Piñuela, L., and García-Ramos, J.C., 2013, Origen de los black shales del Pliensbachiense inferior de la Cuenca Asturiana (España): Revista de la Sociedad Geológica de España, v. 26, no. 1, p. 41–54.

Beroiz, C., Barón, A., Ramírez del Pozo, J., Giannini, G., and Gervilla, M., 1972a, Mapa Geológico de España, Hoja 30 (Villaviciosa): Madrid, Spain, Instituto Geológico y Minero de España, scale 1:50,000.

Beroiz, C., Pignatelli, R., Felgueroso, C., Ramírez del Pozo, J., Giannini, G., and Gervilla, M., 1972b, Mapa Geológico de España, Hoja 29 (Oviedo): Madrid, Spain, Instituto Geológico y Minero de España, scale 1:50,000.

Beroiz, C., Ramírez del Pozo, J., Giannini, G., Barón, A., Julivert, M., and Truyols, J., 1972c, Mapa Geológico de España, Hoja 14 (Gijón): Madrid, Spain, Instituto Geológico y Minero de España, scale 1:50,000.

Carrivick, J.L., Smith, M.W., and Quincey, D.J., 2016, Structure from Motion in the Geosciences. Collection of New Analytical Methods in Earth and Environmental Science: Chichester, UK, John Wiley & Sons Ltd., 208 p., https://doi.org/10.1002/9781118895818.

Cawood, A.D., Bond, C.E., Howell, J.A., Butler, R.W.H., and Totake, Y., 2017, LiDAR, UAV or compass-clinometer? Accuracy, coverage and the effects on structural models: Journal of Structural Geology, v. 98, p. 67–82, https://doi.org/10.1016/j.jsg.2017.04.004.

Corsini, M., Cignoni, P., and Scopigno, R., 2012, Efficient and flexible sampling with blue noise properties of triangular meshes: IEEE Transactions on Visualization and Computer Graphics, v. 18, p. 914–924, https://doi.org/10.1109/TVCG.2012.34.

Erslev, E., 1991, Trishear fault-propagation folding: Geology, v. 19, no. 6, p. 617–620, https://doi.org/10.1130/0091-7613(1991)019<0617:TFPF>2.3.CO;2.

Fonstad, M.A., Dietrich, J.T., Courville, B.C., Jensen, J.L., and Carbonneau, P.E., 2013, Topographic structure from motion: A new development in photogrammetric measurement: Earth Surface Processes and Landforms, v. 38, p. 421–430, https://doi.org/10.1002/esp.3366.

García-Ramos, J.C., and Gutiérrez Claverol, M., 1995, La cobertera mesozoico-terciaria, *in* Aramburu, C., and Bastida, F, eds., Geología de Asturias: Gijón, Spain, Ediciones Trea, Gijón, p. 81–94.

García-Ramos, J.C., Suárez de Centi, C., and Valenzuela, M., 1992, Icnofósiles, sedimentación episódica, tempestitas fangosas y "black shales" de ambientes seudoanóxicos, en sucesiones marinas de plataforma y rampa: Geogaceta, v. 12, p. 99–100.

García-Ramos, J.C., Piñuela, L., and Rodríguez-Tovar, F.J., 2001, XI International Ichnofabric Workshop Field Trip Guidebook: Colunga, Spain, 89 p.

García-Ramos, J.C., Piñuela, L., Aramburu, C., Suárez-Ruiz, I., and Ruiz-Omeñaca, J.I., 2008, Asturian Jurassic Coast: International Conference on Coal and Organic Petrology, Field Trip Guidebook: Oviedo, Spain, 44 p.

Gervilla, M., Beroiz, C., Pignateli, R., Baron, A., Coma, J.E., Felgeroso, C., Ramírez del Pozo, J., and Giannini, G., 1973a, Memoria del Mapa Geológico de España, Escala 1:50,000, Hoja 29 (Oviedo): Madrid, Spain, Instituto Geológico y Minero de España, 64 p.

Gervilla, M., Beroiz, C., Pignateli, R., Baron, A., Coma, J.E., Felgeroso, C., Ramírez del Pozo, J., and Giannini, G., 1973b, Memoria del Mapa Geológico de España, Escala 1:50,000, Hoja 30 (Villaviciosa): Madrid, Spain, Instituto Geológico y Minero de España, 54 p.

Julivert, M., Ramírez del Pozo, J., and Truyols, J., 1971, Le reseau de failles et la couverture post-Hercynienne dans les Asturies, *in* Histoire Structurale du Golfe de Gascogne, Volume 2: Paris, Ed. Technip, p. V3-1–V3-33.

Julivert, M., Truyols, J., Ramírez del Pozo, J., and Giannini, G., 1973, Memoria del Mapa Geológico de España, Escala 1:50,000, Hoja 14 (Gijón): Madrid, Spain, Instituto Geológico y Minero de España, 48 p.

Lepvrier, C., and Martínez-García, E., 1990, Fault development and stress evolution of the post-Hercynian Asturian Basin (Asturias and Cantabria, northwestern Spain): Tectonophysics, v. 184, p. 345–356, https://doi.org/10.1016/0040-1951(90)90447-G.

Lockley, M.G., Lires, J., García-Ramos, J.C., Piñuela, L., and Avanzini, M., 2007, Shrinking the world's largest dinosaur tracks: Observations on the ichnotaxonomy of *Gigantosauropus asturiensis* and *Hispanosauropus hauboldi* from the Upper Jurassic of Asturias: Ichnos, v. 14, no. 3–4, p. 247–255, https://doi.org/10.1080/10420940601050048.

Martín, S., Uzkeda, H., Poblet, J., Bulnes, M., and Rubio, R., 2013, Construction of accurate geological cross-sections along trenches, cliffs and mountain slopes using photogrammetry: Computers & Geosciences, v. 51, p. 90–100, https://doi.org/10.1016/j.cageo.2012.09.014.

Menéndez Casares, E., González Fernández, B., Gutiérrez Claverol, M., and García-Ramos, J.C., 2004, Precisiones sobre los acuíferos de la cuenca jurásica asturiana (NO de España): Trabajos de Geología, v. 24, p. 119–126.

Odriozola, M., 2016, Análisis Estructural de los Materiales Jurásicos de la Playa de Peñarrubia, Gijón [M.Sc. thesis]: Oviedo, Spain, Universidad de Oviedo, 31 p.
Pello, J., 1967, Estudio geológico de la prolongación del borde oriental de la Cuenca Minera Central de Asturias (NW de España): Trabajos de Geología, v. 1, p. 27–39.
Pignatelli, R., Giannini, G., Ramírez del Pozo, J., Beroiz, C., and Barón, A., 1972, Mapa Geológico de España, Hoja 15 (Lastres): Madrid, Spain, Instituto Geológico y Minero de España, scale 1:50,000.
Pignatelli, R., Giannini, G., Ramírez del Pozo, J., Beroiz, C., and Barón, A., 1973, Memoria del Mapa Geológico de España, Escala 1:50,000, Hoja 15 (Lastres): Madrid, Spain, Instituto Geológico y Minero de España, 25 p.
Poblet, J., and McClay, K., 1996, Geometry and kinematics of single-layer detachment folds: American Association of Petroleum Geologists Bulletin, v. 80, no. 7, p. 1085–1109.
Poblet, J., Muñoz, J.A., Travé, A., and Serra-Kiel, J., 1998, Quantifying the kinematics of detachment folds using three-dimensional geometry: Application to the Mediano anticline (Pyrenees, Spain): Geological Society of America Bulletin, v. 110, no. 1, p. 111–125, https://doi.org/10.1130/0016-7606(1998)110<0111:QTKODF>2.3.CO;2.
Poblet, J., Bulnes, M., Mcclay, K., and Hardy, S., 2004, Plots of crestal structural relief and fold area versus shortening: A graphical technique to unravel the kinematics of thrust-related folds, *in* McClay, K.R., ed., Thrust Tectonics and Hydrocarbon Systems: American Association of Petroleum Geologists Memoir 82, p. 372–399.
Pulgar, J.A., Alonso, J.L., Espina, R.G., and Marín, J.A., 1999, La deformación alpina en el basamento varisco de la Zona Cantábrica: Trabajos de Geología, v. 21, p. 283–295.
Riaza Molina, C., 1996, Inversión estructural en la cuenca mesozoica del off-shore asturiano: Revisión de un modelo exploratorio: Geogaceta, v. 20, no. 1, p. 169–171.
Rodríguez Fernández, L.R., Navarro, D., Leyva, F., Villa, E., Granados, L., García-Ramos, J.C., Valenzuela, M., Suárez de Centi, C., Truyols, J., Sánchez de Posada, L.C., Martínez-Chacón, M.L., Menéndez-Álvarez, J.R., Laveine, J.P., Loboziak, S., Candilier, A.M., Aramburu, C., and Matas, J., 1996, Memoria del Mapa Geológico de España, Escala 1:50,000, Hoja 31 (Ribadesella): Madrid, Spain, Instituto Geológico y Minero de España, 109 p.
Soler, R., López Vilchez, J., and Riaza Molina, C., 1981, Petroleum geology of the Bay of Biscay, *in* Illing, L.V., and Hobson, G.D., eds., Petroleum Geology of the Continental Shelf of North-West Europe: London, UK, London Institute of Petroleum, p. 474–482.
Suárez Rodríguez, A., 1988, Estructura del área de Villaviciosa-Libardón (Asturias, Cordillera Cantábrica): Trabajos de Geología, v. 17, p. 87–98.
Suárez-Ruiz, I., and Prado, J.G., 1995, Characterization of Jurassic black shales from Asturias (northern Spain): Evolution and petroleum potential, *in* Snape, C., ed., Composition, Geochemistry and Conversion of Oil Shales: Dordrecht, Netherlands, Kluwer Academic Publishers, p. 387–393, https://doi.org/10.1007/978-94-011-0317-6_24.
Suárez Vega, L.C., 1974, Estratigrafía del Jurásico de Asturias: Cuadernos de Geología Ibérica, v. 74, no. 3, p. 1–369.
Suppe, J., and Medwedeff, D.A., 1990, Geometry and kinematics of fault-propagation folding: Eclogae Geologicae Helvetiae, v. 80, no. 3, p. 409–454.
Triggs, B., McLauchlan, P.F., Hartley, R.I., and Fitzgibbon, A.W., 2000, Bundle adjustment—A modern synthesis, *in* Triggs, B., Zisserman, A., and Szeliski, R., eds., Vision Algorithms: Theory and Practice: Berlin, Germany, Springer-Verlag, p. 298–372, https://doi.org/10.1007/3-540-44480-7_21.
Uzkeda, H., 2013, Reconstrucción 3D y Análisis Estructural de las Rocas Jurásicas de Colunga-Tazones (Cuenca Asturiana, NO de la Península Ibérica) [Ph.D. thesis]: Oviedo, Spain, Universidad de Oviedo, 244 p.
Uzkeda, H., Poblet, J., and Bulnes, M., 2010, A geometric and kinematic model for double-edge propagating thrusts involving hangingwall and footwall folding. An example from the Jaca–Pamplona Basin (Southern Pyrenees): Geological Journal, v. 45, no. 5–6, p. 506–520, https://doi.org/10.1002/gj.1205.
Uzkeda, H., Bulnes, M., Poblet, J., García-Ramos, J.C., and Piñuela, L., 2013, Buttressing and reverse reactivation of a normal fault in the Jurassic rocks of the Asturian Basin, NW Iberian Peninsula: Tectonophysics, v. 599, p. 117–134, https://doi.org/10.1016/j.tecto.2013.04.012.
Uzkeda, H., Bulnes, M., Poblet, J., García-Ramos, J.C., and Piñuela, L., 2016, Jurassic extension and Cenozoic inversion tectonics in the Asturian Basin, NW Iberian Peninsula: 3D structural model and kinematic evolution: Journal of Structural Geology, v. 90, p. 157–176, https://doi.org/10.1016/j.jsg.2016.08.003.
Valenzuela, M., 1988, Estratigrafía, Sedimentología y Paleogeografía del Jurásico de Asturias [Ph.D. thesis]: Oviedo, Spain, Universidad de Oviedo, 748 p.
Valenzuela, M., García-Ramos, J.C., and Suárez de Centi, C., 1986, The Jurassic sedimentation in Asturias (N Spain): Trabajos de Geología, v. 16, p. 121–132.
Wu, C., 2013, Towards linear-time incremental structure from motion, *in* Proceedings of the 2013 International Conference on 3D Vision (3DV 2013): Institute of Electrical and Electronics Engineers (IEEE) Computer Society, Conference Publishing Services, p. 127–134.
Wu, C., Agarwal, S., and Curless, B., Seitz and S.M., 2011, Multicore bundle adjustment, *in* Proceedings of the 2011 IEEE Conference on Computer Vision and Pattern Recognition (CVPR): Institute of Electrical and Electronics Engineers (IEEE) Computer Society, Conference Publishing Services, p. 3057–3064.